The syncollisional granitoid magmatism and crust growth during the West Qinling Orogeny, China: Insights from the Jiaochangba pluton

Juanjuan Kong [a, b, c] *, Yaoling Niu [a, b, d,e] *, Meng Duan [e], Fengli Shao [a, b, c], Yuanyuan Xiao [a, b], Yu Zhang [b], Pengyuan Guo [a, b], Pu Sun [a, b, c], Hongmei Gong [a, b]

[a] Institute of Oceanology, Chinese Academy of Sciences, Qingdao 266071, China

[b] Laboratory for Marine Geology, Qingdao National Laboratory for Marine Science and Technology, Qingdao 266061, China

[c] University of Chinese Academy of Sciences, Beijing 100049, China

[d] Department of Earth Sciences, Durham University, Durham DH1 3LE, UK

[e] School of Earth Science and Resources, China University of Geosciences, Beijing 100083, China

*Corresponding authors:
Miss Juanjuan Kong, juanjuan0317@foxmail.com
Professor Yaoling Niu, yaoling.niu@durham.ac.uk

Address: Institute of Oceanology, Chinese Academy of Sciences, 7 Nanhai Road, Qingdao 266071, China. Tel.: +86 0532 82898980

Abstract

The West Qinling Orogenic Belt (WQOB) is a major portion of the Qinling-Dabie-Sulu Orogen and holds essential information for understanding the protracted evolution of the northeastern branch of the Paleo-Tethys in East Asia. In this study, we report our petrological, geochemical and geochronological study on the five Triassic granitoid plutons of West Qinling with emphasis on the poorly studied Jiaochangba pluton with zircon U-Pb ages of 217.5 ± 1.6 Ma and 215.2 ± 1.2 Ma. The new data and the existing data on the other four plutons support the view that the West Qinling granitoids represent a magmatic response to the continental collision of the Yangtze Block (YB) with the North China Craton (NCC) in the Triassic. Like the other four plutons, the Jiaochangba pluton show strong light rare earth element (REE) enrichment and weak heavy REE depletion ($[La/Sm]_N \approx 7.14 \pm 1.89$; $[Sm/Yb]_N \approx 4.63 \pm 1.85$) with varying negative Eu anomalies ($Eu/Eu^* \approx 0.65 \pm 0.20$). In the N-MORB normalized diagram, all the samples show relative enrichment in Rb, Pb, U and K with negative Nb, Ta, P and Ti anomalies, resembling those of the model continental crust. The Jiaochangba pluton has relatively lower $(^{87}Sr/^{86}Sr)_i$ (0.7062 to 0.7081), higher $\varepsilon_{Nd}(t)$ (-6.91 to -2.09) and $\varepsilon_{Hf}(t)$ (-5.57 to -0.14) than mature continental crust, which are consistent with their source being dominated by lower crust with significant mantle contributions. Mantle-derived melt, which formed from partial melting of mantle wedge peridotite facilitated by dehydration of the subducted/subducting Mianlue ocean crust, provide the required heat for the crustal melting while also contributing to the compositions of these granitoids. Evolution of such parental magmas in open system crustal magma chambers with continued evolution/replenishment and crustal contamination and assimilation give rise to

59 the observed petrological and geochemical characteristics of these granitoids.

60 ***Keywords***: continental collision; Jiaochangba granitoids; lower crust melting; petrogenesis;
61 West Qinling

62

63 1. Introduction

64 It has been accepted that the bulk continental crust (BCC) has grown progressively
65 through episodic magmatism over Earth's history (Condie, 2000). Granites are the most
66 abundant igneous rocks in the Earth's upper continental crust. Hence, granitic magmatism
67 has been widely used to study continental crust growth. Traditionally, continental crust is
68 considered to be formed through subduction-zone magmatism because of the arc-like
69 chemical signature of the BCC (e.g., enrichment of large ion lithophile elements (LILEs),
70 depletion in high field strength elements (HFSEs)), which is termed "island arc model"
71 (Taylor, 1967). However, the "island arc model" has more difficulties than certainties,
72 including, e.g., (1) Bulk arc crust is too mafic for the andesitic bulk continental crust; (2) Arc
73 settings have no net crustal addition (see Niu and O'Hara, 2009; Niu et al., 2013). Because
74 of this and on the basis of their detailed studies of the Linzizong syncollisional volcanic
75 sequence in southern Tibet (Niu et al., 2007; Mo et al., 2008), Niu and co-workers
76 hypothesize that continental collision zones are primary sites of net continental crustal
77 growth (Niu et al., 2013). In this hypothesis, during continental collision, the remaining
78 subducted ocean crust undergoes partial melting under amphibolite facies conditions, which
79 produces and preserves granitoid magmas, contributing to net growth of continental crust.
80 Because globally, active seafloor subduction is continuous, but continental collision is

episodic, this hypothesis also satisfies the episodic growth of the continental crust and overcomes the difficulties of "island arc model". This hypothesis has been tested with success along several orogenic belts on the greater Tibetan Plateau (Mo et al., 2007; Mo et al., 2008; Niu and O'Hara, 2009; Niu et al., 2013; Huang et al., 2014; Chen et al., 2015; Zhang et al., 2016; Shao et al., 2017).

In this paper, we further test this hypothesis on syncollisional granitoids in the West Qingling Orogenic Belt (WQOB) by (1) presenting new LA-ICP-MS zircon U-Pb ages, whole-rock major and trace element data and Sr-Nd-Hf isotopic compositions for the syncollisional Jiaochangba (JCB) pluton, and (2) discussing the petrogenesis of the JCB granitoid pluton together with the four other coexisting granitoid plutons in space and time (i.e., Luchuba, Wuchaba, Lvjing, Baijiazhuang and JCB,).

The WQOB is the western segment of the Qinling orogenic belt in central China, which is one of the largest in Asia (Mattauer et al., 1985), linking Kunlun and Qilian orogens to the west and Dabie-Sulu orogen to the east (Lai et al., 1996; Meng and Zhang, 2000; Ratschbacher et al., 2003). The Qinling orogen is a multistage orogen with two sutures. The northern suture lies along the Shangdan tectonic zone, whereas the southern suture is marked by the Mianue ophiolite complex. The Qinling orogen developed through a series of complex seafloor subduction and terrene collision events (Zhang et al., 2001; Ratschbacher et al., 2003;

101 Wang et al., 2009; Wu and Zheng, 2012; Dong et al., 2015), ultimately completed as a result
102 of the continental collision of the Yangtze Block (YB) with the North China Craton (NCC)
103 along the Mianlue suture zone in the Triassic (see Figure 1; Dong et al., 2011 and references
104 therein). Abundant granitoids were produced in West Qinling this time and have received
105 much attention in recent decades with mounting geochronological and geochemical data with
106 the aim of better understanding magma sources and processes in the context of studying the
107 Qinling orogenesis. However, the petrogenesis of these granitoids remains controversial, e.g.,
108 magma mixing of mantle-derived basaltic magmas and crust-derived felsic magmas or lower
109 crust melting (e.g., Sun et al., 2002; Qin et al., 2009, 2010; Jiang et al., 2010; Liu et al., 2011a,
110 b; Dong et al., 2011, 2012; Yang et al., 2011, 2012; Zhu et al., 2013; Xiao et al., 2014; Liang
111 et al, 2015; Li et al., 2017).

112 ## 2. Geological setting and sampling

113 The Qinling orogen has been divided into East and West Qinling on the basis of their
114 geology (Zhang et al., 2001, 2005, 2007; Feng et al., 2002; Figure 1b). The west Qinling
115 orogenic belt is adjacent to the Qilian orogenic belt (Figure 1a) and is bounded by the
116 Wushan-Tianshui fault to the north and the Mianlue suture to the south (Figure 1b). The
117 granitoids are mainly of Indosinian age distributed along the north of the Mianlue suture (Zhu
118 et al., 2011). In the WQOB, the Phanerozoic stratigraphy is dominated by the Devonian-
119 Cretaceous sedimentary sequences with minor Cambrian-Silurian sedimentary series (Feng
120 et al., 2002). The JCB pluton located in the center of the WQOB is circular in shape and
121 covers ~120 km^2 in area, and intruded the Permian strata (Figure 1c). We collected samples
122 from the JCB pluton (104°37′31.0″-104°38′29.0″E, 34°26′21.3″-34°30′35.4″N) and its

surrounding plutons (i.e., Luchuba, Wuchaba, Lvjingand Baijiazhuang; Figure 1c). The Luchuba, Wuchaba, Lvjing and Baijiazhuang plutons nearly all comprise diorites, quartz diorites, granodiorites and monzogranites with varying amount of mafic magmatic enclaves (MMEs) (Duan et al., 2016; Kong et al., 2017; Yang et al., 2017). The lithology, geochemistry, geochronology and general characteristics of the five granitoid plutons including JCB pluton are given in Table 1.

The granitoid samples from the JCB pluton are intermediate- to coarse-grained biotite granites with gray to pink colors and granitic texture (Figure 2a). Their mineralogy includes K-feldspar (~ 20%), plagioclase (~ 35%), quartz (~ 30%) and minor hornblende and biotite (~ 5%) with accessory apatite, zircon and Fe-Ti oxides (Figure 2c). Fine-grained mafic magmatic enclaves (MMEs) are dispersed in the JCB pluton (Figure 2b). The MMEs are of fine-grained granitic texture dominated by hornblende + biotite (~ 40% in total), plagioclase (~ 40%) and quartz (~ 15%) with accessory minerals similar to those in their granitoid host (Figure 2d). Figure 2d shows the sharp contact of MMEs with their host granodiorite, where MMEs are finer-grained than the host and have no chilled margins and textures of crystal resorption and reactive overgrowth. Mafic minerals and plagioclase are generally euhedral to subhedral, indicating that they may represent early-formed phases (see Reid and Hamilton, 1987); some plagioclase crystals showing clear zoning with K-feldspar and quartz being interstitial..

3. Analytical methods

Ten freshest and representative samples from the JCB pluton were analyzed for whole-

144 rock major and trace elements, and Sr-Nd-Hf isotope compositions. Two of the samples were
145 selected for zircon U-Pb dating. Weathered surfaces and pen saw marks were removed and
146 thoroughly cleaned, then ultrasonically cleaned with Milli-Q water and dried before
147 powdered using an agate mill into ~ 200-mesh in a clean environment.

148 ***3.1 LA-ICP-MS zircon U-Pb dating***

149 Zircons were extracted using combined techniques of heavy liquid and magnetic
150 separation. The zircon internal structure was examined using cathodoluminescence (CL)
151 imaging on an EMPA-JXA-8100 scanning electron microscope at China University of
152 Geosciences, Wuhan (CUGW). Zircon U-Pb dating on samples JCB12-07 and JCB12-12 was
153 carried out at the Geological Lab Center, China University of Geosciences, Beijing (CUGB)
154 using an Agilent 7500a inductively coupled plasma mass spectrometry (ICP-MS) with a New
155 Wave UPP-193 laser ablation system. During the analysis, laser spot size was set to ~ 36 μm
156 for most analyses and to 25 μm for some rims, laser energy density at 8.5 J/cm^2 and repetition
157 rate at 10 Hz. The procedure of laser sampling is 5-s pre-ablation, 20-s sample-chamber
158 flushing and 40-s sample ablation. The ablated material is carried into the ICP-MS by the
159 high-purity Helium gas stream with flux of 0.8 L/min. The whole laser path was fluxed with
160 N_2 (15 L/min) and Ar (1.15 L/min) in order to increase energy stability. Calibrations were
161 done using NIST 610 glass as an external standard and Si as an internal standard. U-Pb
162 isotope fractionation effects were corrected for using zircon 91500 (Wiedenbeck et al., 1995)
163 as an external standard. The age data processed using the GLITTER4.41 program are given
164 in Table 2 with analytical details given in Song et al. (2010a). The concordia diagrams and
165 weighted mean age calculation were performed using ISOPLOT 4.15 (Ludwig, 2012; Figure

166 3).

167 ***3.2 Mineral compositions***

168 Mineral chemistry was determined using a JEOL EPMA8230 microprobe at Langfang,
169 China. The analytical procedure follows the quantitative analysis of silicate minerals by
170 electron probe microanalysis of the State Standard of the People's Republic of China (GB/T
171 15617–2002).

172 ***3.3 Major and trace elements***

173 Whole-rock major and trace elements were analyzed using Prodigy Inductively Coupled
174 Plasma Optical Emission Spectrometer (ICP-OES) and Agilent 7500a ICP-MS at CUGB,
175 respectively. Analyses of United States Geological Survey (USGS) rock standards (AGV-2)
176 and Chinese national rock standard (GSR-1 and GSR-3) give precisions (1σ) better than 1%
177 for most major elements, except for TiO_2 (~ 1.5%) and P_2O_5 (~ 2%) and better than 5% for
178 most trace elements, but 10-13% for Cu, Sc, Nb, Er, Th, and U, and between 10% and 15%
179 for Ta, Tm, and Gd (2σ). Analytical details are given in Song et al. (2010b).

180 ***3.4 Sr-Nd-Hf isotopes***

181 The whole-rock Sr-Nd-Hf isotopic compositions of five samples were determined at
182 CUGW following the chemical separation and analysis procedures of Gao et al. (2004) and
183 Yang et al. (2010). The Sr, Nd isotopic analyses were done on a Thermo Finnigan Triton Ti
184 Thermal Ionization Mass Spectrometer (TIMS). The Hf isotopic analysis was done using a
185 Thermo Neptune Plus Multi-Collector Inductively Coupled Plasma Mass Spectrometer (MC-

ICP-MS). The other five samples for Sr-Nd-Hf isotopes were analyzed using MC-ICP-MS in the Institute of Oceanology, Chinese Academy of Sciences (IOCAS), Qingdao. The chemical separation procedures are given in (Sun et al., 2017 in preparation). Analysis of NBS987 standard run during the same period gave $^{87}Sr/^{86}Sr = 0.710254 \pm 13$ (n = 5, 2σ), and $^{143}Nd/^{144}Nd = 0.512109 \pm 6$ (n = 9, 2σ) for JNdi-1 standard. The Alfa Hf international standard yielded a mean $^{176}Hf/^{177}Hf$ of 0.282194 ± 11 (n = 13, 2σ). The values of USGS reference materials AGV-2, GSP-2 and RGM-2 run with our samples are given in Appendix A, which are consistent with the recommended reference values (GeoREM, http://georem.mpch-mainz.gwdg.de/).

4. Results

4.1 Zircon U-Pb age

Zircon grains from the JCB pluton are ~100 to 300 μm in size and have length/width ratio of 1:1 to 3:1 (Figure 3a, b). They have clear oscillatory zoning in the CL images and display varying U (110 to 3319 ppm) and Th (85 to 1240 ppm) with Th/U ratios of 0.16 to 1.12, which are consistent with being of magmatic origin (Rubatto and Gebauer, 2000; Corfu et al., 2003; Hanchar and Hoskin, 2003). Thirteen zircon grains of JCB12-07 give apparent $^{206}Pb/^{238}U$ ages of 216 ± 3 Ma to 221 ± 3 Ma, with a weighted mean age of 217.5 ± 1.6 Ma (MSWD = 0.104, n = 13) (Figure 3a). However, it is noteworthy that some data points plot to the right side of the concordia, probably due to analytical uncertainty of ^{207}Pb and trace common lead (Yuan et al., 2003). Twenty-seven zircons from sample JCB12-12 give a weighted mean $^{206}Pb/^{238}U$ age of 215.2 ± 1.2 Ma (MSWD = 0.17, n = 27) (Figure 3b). These ages represent the emplacement age of the JCB pluton, which are in agreement with the time

208 of the NCC-YB collision (Dong et al., 2012).

209 ***4.2 Mineral compositions***

210 Carefully selected plagioclase and amphibole crystals were analyzed for major element
211 composition using electron microprobe, in which Fe^{2+} and Fe^{3+} values of amphibole were
212 recalculated after Lin and Peng (1994).

213 However, the lack of reversed zoning rules out the magma mixing hypothesis for the
214 petrogenesis of the MMEs and their host granodiorite (Figure 4 and Table 3). Following
215 Leake et al. (1997), amphiboles from the MMEs and their host granodiorite are
216 compositionally the same and can be classified as calcic magnesiohornblende with high $Mg^{\#}$
217 (0.46-0.61) [$Mg^{\#}$=Mg/(Mg+Fe^{2+})] (Figure 5 and Table 3). All the amphibole crystals of the
218 MMEs and their host granodiorite are compositionally uniform without zoning (Table 3).
219 Moreover, the mafic minerals in the MMEs are richer in Mg and plagioclases are more calcic
220 than those of the host (Table 3), support the mafic cumulate model for the MMEs (see Chen
221 et al., 2016, 2018).

222 ***4.3 Major and trace elements***

223 The analytical data for whole-rock major and trace element compositions are given in
224 Table 4. In the total alkalis-silica (TAS) diagram (Figure 6a), the granitoid host samples plot
225 in the granite and granodiorite field and the MME samples plot in the granodiorite and
226 gabbroic diorite field. The samples are compositionally high-K calc-alkaline with high
227 K_2O/Na_2O (0.79 - 1.62 for the host and 1.52 for the MME; Figure 6b) and weak peraluminous
228 to metaluminous with varying A/CNK (0.95 - 1.15 for the host and 0.62 for the MME; Figure
229 6c). On SiO_2-variation diagrams (Figure 7), the granitoids define inverse linear trends for

major elements (e.g., TiO_2, Al_2O_3, TFe_2O_3, MgO, CaO, P_2O_5) and selected trace elements (Sr, Eu and Zr), which are apparently consistent with fractionation of amphibole, biotite and plagioclase, and are more directly controlled by modal mineralogy of the samples. It should also be noted that in the majority of the silica variation diagrams (Figure 7), the JCB MME composition differs significantly from both the host rock and other MMEs compositions for its high mode of mafic minerals.

The JCB granitoid host samples display highly fractionated REE patterns $(La/Yb)_N$ = 3.86 to 48.51, $[La/Sm]_N > 1$, $[Sm/Yb]_N > 1$) and moderate negative Eu anomalies (Eu/Eu* = 0.30 to 0.85) (i.e., weak HREEs depletion, Figure 8). The MME sample shows $(La/Yb)_N$ = 12.96 and Eu/Eu* = 0.80 (Figure 8). The Nb/Ta ratios (10.64 to 17.94 with an average of 14.79) of the host rocks and MME (14.95) are sub-chondritic (chondrite Nb/Ta ratio: 17.5, Sun and McDonough, 1989), even lower than that of upper oceanic crust (16.08, Niu and O'Hara, 2009). In the multi-element diagram, all the samples are enriched in LILEs (e.g., Rb, K, Pb) and relatively depleted in HFSEs (e.g., Nb, Ta, Ti) (Figure 8b). These characteristics resemble those of bulk continental crust (BCC; Rudnick and Gao, 2003).

4.4 Sr-Nd-Hf isotopes

Whole rock Sr-Nd-Hf isotope data for 10 samples (including MME) of the JCB pluton are given in Table 5 and plotted in Figures9 and 12. The $I_{Sr}(t)$, $\varepsilon_{Nd}(t)$ and $\varepsilon_{Hf}(t)$ (where t = 220 Ma) are variable, i.e., $I_{Sr}(t)$ = 0.7062 to 0.7081), $\varepsilon_{Nd}(t)$ = -6.91 to -3.97) and $\varepsilon_{Hf}(t)$ = -5.57 to -1.71. The whole-rock Nd isotopic model ages (T_{DM}) are essentially the same (~1.2-2.3 Ga) as the two stage Hf model ages (T_{DM2} ~ 1.0-2.0 Ga). The MME sample also shows similar

Sr-Nd-Hf isotopic compositions ($I_{Sr}(t)$ = 0.7066, $\varepsilon_{Nd}(t)$ = -2.09, $\varepsilon_{Hf}(t)$ = -0.14) to the host granitoid sample. Sample JCB12-06 of the JCB pluton gives very high $^{87}Sr/^{86}Sr$ of 0.8681 because of the high Rb/Sr ratio ($^{87}Rb/^{86}Sr \sim 55.1$) due to significant plagioclase-dominated fractional crystallization (also low in Ba, P and Ti; see Figure 8b), resulting in high radiogenic ^{87}Sr ingrowth, which makes the calculated $I_{Sr}(t)$ unreliable (Jahn et al., 2000).

5. Discussion

5.1 Roles of Fractional Crystallization

As shown in Figure.9, the JCB granitoids display compositional variations. Apart from the effects of magma source heterogeneity and the extent of melting, crystal fractionation can be important factors contributing to the compositional variations. Therefore, it is necessary to evaluate the potential effect of the fractional crystallization before discussing source characteristics of the JCB granitoids.

As pointed out above, the JCB granitoids slightly decrease in TiO_2, Al_2O_3, TFe_2O_3, MgO, CaO, P_2O_5, Sr and Eu with increasing SiO_2 (Figure 7), likely suggestive of fractional crystallization of ferromagnesian minerals (biotite ± hornblende), plagioclase, Fe-Ti oxides, and apatite (Rollison, 1993). The granitoids exhibit decreasing Zr with increasing SiO_2 (Figure 7), indicating that zircon was saturated and on the liquidus (Li et al., 2007; Zhong et al., 2009). Negative Eu anomalies and depleted Ti, P show that fractional crystallization of plagioclase, Fe-Ti oxides, and apatite is important in the petrogenesis (Figure 8). Positive correlations of CaO with Sr and Eu/Eu* (Figure 10a, b) are consistent with modal plagioclase control in the samples (resulting from either plagioclase accumulation or crystallization

removal). Figure 11 shows that fractionation of K-feldspar, plagioclase and biotite played an important role in the petrogenesis of the JCB granitoids. The granitoids show sub-chondritic Nb/Ta ratio (10.64 to 17.94 with an average of 14.79) and depleted in Nb, Ta in spider diagram resulting from the higher partition coefficient of Nb than Ta during hornblende crystallization ($Kd_{hornblende}$ Nb/Ta = 1.40) (Foley et al., 2002). Therefore, fractional crystallization is important in the petrogenesis of these granitoids.

5.2 Petrogenesis of the JCB pluton

Generally, granitoids are typically divided into I-, S-, A- and M-type in terms of source rock types and petrogenesis (Chappell et al., 1974; Collins et al., 1982; Whalen, 1985). The samples of the JCB pluton have $(^{87}Sr/^{86}Sr)_i$ of 0.7062 to 0.7081, $\varepsilon_{Nd}(t)$ of -6.91 to -3.94 and $\varepsilon_{Hf}(t)$ of -5.57 to -2.66, have no aluminous minerals such as muscovite, tourmaline and garnet, and have mafic mineral assemblage of hornblende and biotite (Figure 2). All these, plus relatively low A/CNK values (<=1.1, Figure 6c), are consistent with most of these granitoids being of I-type granitoid.

The earlier study proposed two models to explain the origin of the JCB granitoids pluton: (1) mixing of mafic and felsic magmas on the basis of Sr and O isotopes (Wen et al., 2008); (2) melting of upper crustal argillaceous rocks (Peng, 2013) by interpreting the trace element data, but we consider that these interpretations are problematic (see below).

The JCB pluton contains MMEs. The origin of the MMEs is a key to the petrogenesis of the granitoids and has been the subject of debate (Barbarin, 2005; Chappell et al., 2000; Yang et al., 2007; Niu et al., 2013; Huang et al., 2014; Chen et al., 2015, 2016, 2018). Here,

293 we discuss the MMEs of the five syn-collision granitoid plutons (JCB, Luchuba, Wuchaba,
294 Lvjing and Baijiazhuang) (See Figure 1) (Duan et al., 2016; Kong et al., 2017). Several lines
295 of evidence favoring the mafic cumulate model are addressed below: (1) the petrography
296 shows typical magmatic textures (Figure 2d), ruling out the MMEs being of restite; (2) The
297 MMEs don not show core-to-rim mineral compositional and textural variations, excluding
298 MEEs being of matasonatic origin (Figure 2d) (Eberz et al., 1990). (3) the MMEs have the
299 same mineraly as the host granitoids, but have higher modal amphibole (and biotite). Note
300 that the MMEs have high Cr and Ni contents, consistent with high partition coefficients of
301 Cr and Ni for amphibole and biotite (Ewart et al., 1994); (4) the MMEs have the same age as
302 their host (Jiang, 2016); (5) their different major and trace element abundances from their
303 hosts are largely controlled by mineral modal proportions (Figures 7 and 8); (6) MMEs have
304 slightly higher $\varepsilon_{Nd}(t)$, $\varepsilon_{Hf}(t)$ than their host granitoids and similar $(^{87}Sr/^{86}Sr)_i$ (Figure 9).
305 Obviously, the data are more consistent with the same mantle source with varying extents of
306 crustal contamination (Figure 9a, b, c). The MMEs are less contaminated because they are
307 earlier cumulate whereas the remaining magma continues to evolve and assimilate with the
308 crustal country lithologies before solidified as the granitoid hosts. This is a straightforward
309 geological process (Niu et al., 2013; Chen et al., 2015). It is worthy to note that the bulk
310 composition of the JCB-MME sample is gabbroic diorite (lack of pyroxene) which is
311 different from the granodioritic compositions of other MMEs because of it contains more
312 hornblende. Importantly, the MMEs comprise dominantly amphibole and plagioclase (Figure
313 2d), which are common cumulate minerals in andesitic melts. If the parental melts were
314 basaltic, the typical cumulate from such evolved basaltic melt would be gabbro dominated

315 by clinopyroxene and plagioclase. This is an important petrological concept. It is worth to
316 note that the same or very similar observations mentioned above have been commonly used
317 as evidence for magma mixing for MME-bearing granitoids. Many researchers (e.g. Pin et
318 al., 1990; Holden et al., 1991; Poli and Tommasini, 1991; Elburg, 1996) have claimed partial
319 or complete isotopic equilibration of the MMEs with their host. Experiments show that the
320 isotopic equilibration advances faster than the chemical equilibration and Sr isotopic
321 equilibrium is faster than that of Nd (e.g. Holden et al., 1987; Pin et al., 1990). Compared to
322 the Nd, the Sr isotopic compositions of the host and enclaves are more likely to be
323 equilibrated through diffusion exchange, but it is physically unlikely with isotopes being
324 homogenized whereas major and trace elements are not. Therefore, we maintain that the
325 MMEs are early cumulate as the host granitoids.

326 In the eastern segment of the south Qinling tectonic unit, there are widespread
327 Precambrian basement exposures, e.g., the Yudongzi Group, the Foping Group, the Douling
328 Group, the Wudang Group, the Yaolinghe Group and the Yunxi Group. Their formation time
329 is from the Neoarchean, Paleoproterozoic to Neoproterozoic based on geochronology (Zhang
330 et al., 2002). According to Nd isotopic compositional comparison between the WQOB
331 granitoids and the Precambrian basements of the South Qinling, none of the basements can
332 be taken as the magma source for the WQOB granitoids (Zhang et al., 2007). The JCB pluton
333 has lower and constant $(^{87}Sr/^{86}Sr)_i$, higher $\varepsilon_{Nd}(t)$ and $\varepsilon_{Hf}(t)$ than the mature continental crust
334 ($[^{87}Sr/^{86}Sr]_i < 0.72$, $\varepsilon_{Nd}(t) > -12$) (the reference data are from Niu and O'Hara, 2009).
335 Obviously, it is unlikely that these granitoids were produced by melting mature continental
336 crust, but has significant mantle contribution (or juvenile continental crust) in terms of

337 isotopes. In addition, the slightly radiogenic Hf-Nd isotopes are coupled and lie in the global
338 mantle and crustal array (Figure 9d), and removed far away from (higher than) mature
339 continental crust, which is again consistent with mantle input, reflecting the process of
340 juvenile continental crust formation manifested by the petrogenesis of these granitoids. Some
341 studies suggest that amphibolite dehydration of lower crust can produce such magmas (Zhang
342 et al., 2007), yet amphibolite melting preferentially produces high-Na_2O, not high-K_2O
343 magmas, which are different from the JCB granitoids (Figure 6b; Beard and Lofgren, 1991).
344 Moreover, the chondrite normalized REE patterns (Figure 8a) contradicts with the
345 geochemical signatures formed by partial melting of lower crustal garnet amphibolite or
346 eclogite. Thus, the origin by only partial melting of the pre-existing lower crust is unlikely.

347 To produce such andesitic to felsic BCC-like magmas with inherited mantle-like
348 isotopic composition, it requires a basaltic source plus continental materials. The "island arc"
349 model can produce the "continental signature" (e.g., enriched in LREEs and LILEs, depleted
350 in HFSEs) and mantle-like isotopes. However, the bulk arc crust is too mafic to produce the
351 more felsic melts (Niu et al., 2013). Although Lee and Anderson (2015) offered a solution to
352 this difficulty, partial melting of arc crust will produce high Sr magmas, yet the Sr of the JCB
353 plutons is not as high as island arc basalts (IAB), but only slightly higher than MORB (Niu
354 and O'Hara, 2009) The plagioclase separation can lead to low Sr but it cannot reduce the
355 high Sr/Sr* values in IAB (See Fig. 4 in Niu et al., 2013). Thus, this model is inadequate to
356 explain the JCB pluton in the WQOB. Although the exact timing of the YB with the NCC
357 collision is also controversial, when the paleogeographic evolution is taken into account, the
358 sedimentary facies change from turbiditic deposits during the Early-Middle Triassic to

359 shallow marine-terrestrial deposits during the Middle-Late Triassic in WQOB (Yan et al.,
360 2012). Furthermore, the lack of Late Triassic sedimentary rocks in the South Qinling belt
361 suggests that the Mianlue oceanic basin has been closed during the Late Triassic (Yang et al.,
362 2012). Therefore, the Late Triassic (~ 210-220Ma) magmatism witnessed a period of
363 continental collision. In addition, Mo et al. (2008) already demonstrate that syn-collisional
364 magmatism is capable to produce volumetrically significant I-type granitoid plutons.
365 Therefore, we suggest the JCB pluton formed in a syncollisional setting. The popular
366 explanation is that a thermal pulse associated with slab breakoff resulted in the asthenosphere
367 upwelling along the Mianlue suture during the Late Triassic, and the upwelling
368 asthenosphere triggered partial melting of the Neoproterozoic sub-continental lithosphere
369 mantle (SCLM) that generated the mafic magma and the partial melting of the Neo-
370 Mesoproterozoic lower crust that generated the granitic magmatism (Qin et al., 2009; Zhu et
371 al., 2013; Yang et al., 2015). As noted above, only lower crust melting is unlikely to produce
372 the observed granitoids, and the MMEs as the magmatic cumulate of hornblende-plagioclase
373 assemblage cannot represent mafic magma of SCLM origin, because the asthenosphere
374 mantle cannot upwell and melt upper crust to generate granitic magmas (Wen et al., 2008)
375 without complete lithosphere removal (delamination). Importantly, the popular slab-breakoff
376 model in explaining syncollisional magmatism is physically unlikely (Niu, 2017). Therefore,
377 mixing of mafic and felsic magmas is unlikely to generate the JCB pluton in dynamics.

378 In this case, a reasonable mechanism in a syncollisional setting proposed by Niu et al.
379 (2013) possibly effective in explaining the petrogenesis of these granitoids. Partial melting
380 of subducted basaltic ocean crust under the amphibolite facies conditions can produce

andesitic melts with inherited mantle isotopic signatures (Niu et al., 2013). Partial melting of oceanic crust cannot generate high K/Na melts, and crust contribution is necessary. Isotopes also require possible contributions of continental crustal materials (see above). The host granitoids and the MME have indistinguishable Sr isotopic compositions and $\varepsilon_{Nd}(t)$ and $\varepsilon_{Hf}(t)$ correlated with SiO_2 (Figure 9a, b, c), manifesting significant crustal contamination of these granitoids. The $\varepsilon_{Nd}(t)$ and $\varepsilon_{Hf}(t)$ and SiO_2 of MMEs of JCB, Luchuba, Wuchaba, Lvjing and Baijiazhuang are weakly positively correlated, suggesting the contamination of cumulate samples (MMEs) after their separation from the main body of largely liquid magma (parent magmas) (Reiners et al., 1996), which accords with the cumulate origin of the MMEs (see above). Crustal assimilation with concurrent fractional crystallization (AFC) is now widely considered as an important process of magma evolution (DePaolo et al., 1981). AFC or fractional crystallization (FC) of basaltic magma can produce granitoids (Bowen, 1928). These suggest that the AFC from parental magmas of basaltic or more likely mafic andesitic compositions may be a suitable mechanism for the JCB granitoids. Hence, partial melting of subducted basaltic ocean crust under the amphibolite facies in combination with magma evolution through AFC processes can explain the petrogenesis of the JCB pluton. But simple isotopic calculations show only ~40- 45% ocean crust (MORB) contribution (the maximum contribution) to the source of these granitoids (Figure 12). In the calculation, the Mianlue oceanic crust slab is represented by the 350 Ma ophiolitic MORB in Qinling, central China (Xu et al., 2002), and upper crust is represented by the average composition of ~2000Ma Douling gneiss in South Qinling (Shen et al., 1997). 55-60% mature continental crust contribution likely means the melting occurred at crust depth. MORB melting model cannot

reasonably explain the petrogensis of JCB granitoids. The whole-rock Nd isotopic model ages (T_{DM}; 1.2-2.3 Ga) and two stage Hf model ages (T_{DM}; 1.0-2.0 Ga) of JCB granitoids support a source composed of ancient lower continental crust (Qin et al., 2009). Therefore, we propose a more reasonable model that is consistent with the observations and basic petrological concepts. When the Mianlue oceanic slab subducted beneath the Qinling Block, dehydration of the ocean crust can effectively lower the solidus of mantle wedge peridotite to melt for the basaltic melt (e.g., Pearce and Peate, 1995). Extraction, ascent and underplating of such mantle wedge-derived basaltic melts can induce the lower continental crustal melting to produce magmas parental to the JCB granitoids (Figure 13). All these processes are likely taking place in an open system with continued evolution/replenishment accompanied by crustal contamination and assimilation. Such mantle derived melt, also contributes materials to the granitoid magmatism, i.e., there exists mixing between the mantle-derived isotopically depleted melt and isotopically enriched felsic melt from the lower continental crust, which is consistent with variable isotope compositions (Figure 9). Here, we emphasize that components from depleted mantle wedge and upper crust materials must have been involved in the formation process of the granitic magmas. When a primitive magma body is emplaced into a cold environment with the wall rock having temperatures below the liquidus of the magma, magma quench and rapid crystallization are inevitable because of the thermal contrast, despite the high viscosity of granitoids. The first major liquidus phases of parental magma of the grantoids would be amphibole, biotite, plagioclase, and rapid quench will facilitate abundant nucleation without between-nuclei space for growth, thus forming fine-grained MME cumulate, which can be readily disturbed by replenishing

425 magmas, leading to the dispersed MMEs (Chen et al., 2015, 2016, 2018) in the granitoid
426 hosts. If the parental magmas represent early batches of melt intruding the crustal magma
427 chamber, it would have been assimilated more of the crust materials with evolved Sr isotopic
428 compositions inherited in the cumulated MMEs.

429 ***5.3 The origin of granitoids in West Qinling***

430 The JCB, Luchuba, Wuchaba, Lvjing and Baijiazhuang, all the five plutons are clustered
431 together (Figure 1) commonly called "the Zhongchuan pluton group" in the WQOB (Peng,
432 2013). The genetic relationship of the five plutons remains poorly known (Li et al., 1993; Xu
433 et al., 2006; Peng, 2013). The JCB pluton and the other four syncollisional plutons (Luchuba,
434 Wuchaba, Lvjing and Baijiazhuang) (Duan et al., 2016; Kong et al., 2017) (Figure 1) have
435 MMEs and show similar mineralogy (Qz + Pl + Kfs + Bt ± Hb ± Zircon ± Apatite ± Fe-Ti
436 oxides) with varying modes. They are metaluminous to weakly peraluminous I-type or S-
437 type granitoids and largely belong to high-K calc-alkaline series (Figure 6). These granitoids
438 have similar REE patterns with LREEs enrichment, significant Eu anomalies and trace
439 element patterns resembling those of BCC (Figure 8) and show the similar Sr-Nd-Hf isotope
440 characters with inherited mantle-like isotopic signatures from the mantle wedge (Figure 9),
441 the large Nd-Hf isotope ranges due to the magmas underwent various degrees crustal
442 contamination. Importantly, they have the same intrusive ages (Table 1), all these indicating
443 they are products of the same thermal and tectonic event.

444 ***5.4 Significance of continental crust growth in the WQOB***

445 In our study, trace element patterns of the JCB, Luchuba, Wuchaba, Lvjing and

446 Baijiazhuang plutons resemble those of BCC. Despite the more felsic and radiogenic Sr
447 compositions of the five granitoid plutons, it has relatively higher $\varepsilon_{Nd}(t)$ and $\varepsilon_{Hf}(t)$ than that
448 of mature continental crust ($[^{87}Sr/^{86}Sr]_i < 0.72$, $\varepsilon_{Nd}(t) > -12$) (Niu and O'Hara, 2009). In
449 particular, the value of $\varepsilon_{Nd}(t)$ and $\varepsilon_{Hf}(t)$ of these granitoids obviously higher than the value of
450 continental crust (see Figure 9d and Figure 12), pointing to the contributions of mantle or
451 juvenile crust materials (see Section 5.2). Hence, this syn-collisional pluton represents
452 juvenile crust with primary materials coming from the mantle wedge rather than oceanic crust
453 slab.

454 ***5.5 Tectonic Significance***

455 Our new data also give insights into the evolution of the Qinling Orogen. The detailed
456 geochronological data for the high-pressure/ultrahigh-pressure (HP/UHP) metamorphic
457 rocks manifested that the subduction and continental collision between the NCC and YB took
458 place no later than ca. 230 Ma in the Dabie-Sulu orogen (Liu et al., 2004; Zheng et al., 2008).
459 In comparison, our studied granitoids in the Qinling region represent the initial stage of the
460 NCC-YB continental collision after ~ 220 Ma, which were later than the continental collision
461 age in the Dabie-Sulu Orogen (~ 230 Ma). Our results show that subduction of the Mianlue
462 oceanic crust beneath the WQOB was still going on before ~ 220 Ma and the final closure of
463 the Mianlue oceanic basin occurred at~ 220 Ma. Considering the Paleo-Tethyan Mianlue
464 oceanic basin between the NCC and the YB in the Dabie-Sulu Orogen closed ~ 10 Myrs
465 earlier than that in the Qinling Orogen.

466 **6. Conclusions**

(1) Zircon U-Pb dating yields ages of 217.5 ± 1.6 Ma and 215.2 ± 1.2 Ma for the JCB pluton, essentially the same as the ages of other four plutons in the area. We interpret this magmatism as response to the collision of the Yangtze Block with the North China Craton.

(2) The granitoids of the JCB, Luchuba, Wuchaba, Lvjing and Baijiazhuang plutons display an enriched LILEs and LREE pattern and have variably strong negative Eu anomalies, which is similar to those of bulk continental crust but more evolved. The enriched Sr-Nd-Hf isotope compositions suggest that their main source is the ancient lower continental crust. However, components from depleted mantle wedge and upper crust materials must have been involved in the petrogenesis of the granitic magmas.

(3) We suggest that oceanic crust slab dehydration induced mantle wedge melting remains the primary mechanism for mantle derived basaltic melts, whose underplating and intrusion of the crust can cause continental crustal melting.

(4) Jiaochangba, Luchuba, Wuchaba, Lvjing and Baijiazhuang plutons are products of the same thermal and tectonic event.

Acknowledgements

The research is supported by NSFC (grants: 41130314, 41630968) and Qingdao National Laboratory (grants: U1606401, 2015ASKJ03). We thank Shuo Chen, Huixia Cui, Zhenxing Hu, Jiyong Li, Jinju Liu, Yuxin Ma, Wenli Sun, Xiaohong Wang, Lei Ye, Xiaolu Ye and Guorui Zhang for assistance with sample preparation. We particularly thank Su Li for major and trace analysis and zircon analysis, Zhou Lian for Sr-Nd-Hf isotope

analysis. We also thank Sun-Lin Chung and two anonymous reviewers for their constructive comments and suggestions on the early manuscript improvement.

Disclosure statement

No potential conflict of interest was reported by the authors.

References

Andersen, T. (2002). Correction of common lead in U–Pb analyses that do not report ^{204}Pb. Chemical Geology, 192, 59-79.

Barbarin, B. (2005). Mafic magmatic enclaves and mafic rocks associated with some granitoids of the central Sierra Nevada batholith, California: nature, origin, and relations with the hosts. Lithos, 80, 155-177.

Beard, J. S., Lofgren, G. E. (1991). Dehydration melting and water-saturated melting of basaltic and andesitic greenstones and amphibolites at 1, 3 and 6.9 kb. Journal of Petrology, 32, 465-501.

Blichert-Toft, J., Chauvel, C., Albarède, F. (1997). Separation of Hf and Lu for high-precision isotope analysis of rock samples by magnetic sector-multiple collector icp-ms. Contributions to Mineralogy and Petrology, 127(3), 248-260.

Bowen, N. L. (1928). The evolution of igneous rocks. Science Progress, (1894-1898) 1(2), 152-165.

Chappell, B.W., White, A.J.R. (1974). Two contrasting granite types. Pacific geology, 8(2),

509 173-174.
510 Chappell, B.W., White, A.J.R., Williams, I.S., Wyborn, D., Wyborn, L.A.I. (2000). Lachlan
511 Fold Belt granites revisited: high- and low-temperature granites and their implications.
512 Australian Journal of Earth Sciences, 47, 123-138.
513 Chen, Y.D., Price, R.C., White, A.J.R., Chappell, B.W. (1989). Inclusions in three S-type
514 granites from southeastern Australia. Journal of Petrology, 30, 1181-1218.
515 Chauvel, C., Lewin, E., Carpentier, M., Arndt, N.T., Marini, J.C. (2008). Role of recycled
516 oceanic basalt and sediment in generating the Hf-Nd mantle array. Nature Geoscience,
517 1, 64-67.
518 Condie, K.C. (2000). Episodic continental growth models: Afterthoughts and extensions:
519 Tectonophysics, 322, 153-162.
520 Chen, S., Niu, Y. L., Sun, W. L., Zhang, Y., Li, J. Y., Guo, P. Y., Sun, P. (2015). On the origin
521 of mafic magmatic enclaves (MMEs) in syn-collisional granitoids: evidence from the
522 Baojishan pluton in the North Qilian Orogen, China. Mineralogy and Petrology, 109(5),
523 577-596.
524 Corfu, F., Hanchar, J.M., Hoskin, P.W.O., Kinny, P. (2003). Altas of zircon textures. Reviews
525 in Mineralogy and Geochemistry, 53, 469-500.
526 Dahlquist, J. (2002). Mafic microgranular enclaves: Early segregation from metaluminous
527 magma (sierra de Chepes), Pampean Ranges, NW Argentina. Journal of South American
528 Earth Sciences, 15, 643-655.
529 Depaolo, D. J. (1981). Trace element and isotopic effects of combined wallrock assimilation
530 and fractional crystallization. Earth and Planetary Science Letters, 53(2), 189-202.

531 Dong, Y.P., Zhang, G.W., Neubauer, F., Liu, X.M., Genser, J., Hauzenberger, C. (2011).
532 Tectonic evolution of the Qinling orogen, China: review and synthesis. Journal of Asian
533 Earth Sciences, 41, 213-237.
534 Dong, Y., Liu, X., Zhang, G., Chen, Q., Zhang, X., Li, W., Yang, C. (2012). Triassic diorites
535 and granitoids in the Foping area: Constraints on the conversion from subduction to
536 collision in the Qinling orogen, China. Journal of Asian Earth Sciences, 47, 123-142.
537 Dong, Y., Zhang, X., Liu, X., Li, W., Chen, Q., Zhang, G., Zhang, F. (2015). Propagation
538 tectonics and multiple accretionary processes of the Qinling Orogen. Journal of Asian
539 Earth Sciences, 104, 84-98.
540 Duan, M., Niu, Y.L., Kong, J.J., Zhang, Y., Hu, Y., Sun, P. (2016). Zircon U-Pb
541 geochronology, Sr-Nd-Hf isotopic geochemistry and geological significance of
542 Baijiazhuang and Lvjing granitic plutons in West Qinling Orogen. Lithos, 260, 443-456.
543 Eberz, G. W., Nicholls, I. A. (1990). Chemical modification of enclave magma by post-
544 emplacement crystal fractionation, diffusion and metasomatism. Contributions to
545 Mineralogy & Petrology, 104(1), 47-55.
546 Elburg, M.A., (1996). Evidence of isotopic equilibration between microgranitoid enclaves
547 and host granodiorite, Warburton Granodiorite, Lachlan Fold Belt, Australia. Lithos, 38,
548 1–22.
549 Ewart, A., Griffin, W.L. (1994). Application of Proton-Microprobe Data to Trace-Element
550 Partitioning in Volcanic-Rocks. Chemical Geology, 117(1-4), 251-284.
551 Feng Y. M., Cao, X.Z., Zhang, E. P., Hu, Y. X., Pan, X. P., Yang, J. L., Jia, Q. Z., Li, W. M.
552 (2002). Structure, orogenic processes and geodynamic of the western Qinling orogen

553 (in Chinese). Xi'an map press, Xi'an, pp 1-263.
554 Foley, S., Tiepolo, M., Vannucci, R. (2002). Growth of early continental crust controlled by
555 melting of amphibolite in subduction zones. Nature, 417, 837-840.
556 Gao, S., Rudnick, R. L., Yuan, H. L., Liu, X. M., Liu, Y. S., Xu, W. L., Ling, W. L., Ayers, J.,
557 Wang, X. C., Wang, Q. H. (2004). Recycling lower continental crust in the North China
558 craton. Nature, 432, 892-897.
559 Griffin, W. L., Wang, X., Jackson, S. E., Pearson, N. J., O'Reilly, S. Y., Xu, X.S., Zhou, X.
560 M. (2002). Zircon chemistry and magma mixing, se china: in-situ analysis of hf isotopes,
561 tonglu and pingtan igneous complexes. Lithos, 61(3), 237-269.
562 Hanchar, J.M., Hoskin, P.W.O. (2003). Zircon. Reviews in Mineralogy and Geochemistry,
563 53, 1-500.
564 Holden, P., Halliday, A. N., Stephens, W. E. (1987). Neodymium and strontium isotope
565 content of microdiorite enclaves points to mantle input to granitoid production. Nature,
566 330(6143), 53-56.
567 Huang, H., Niu, Y. L., Nowell, G., Zhao, Z. D., Yu, X. H., Zhu, D. C., Mo, X. X., Ding, S.
568 (2014). Geochemical constraints on the petrogenesis of granitoids in the East Kunlun
569 Orogenic belt, northern Tibetan Plateau: Implications for continental crust growth
570 through syn-collisional felsic magmatism. Chemical Geology, 370, 1-18.
571 Jahn, B. M., Wu, F. Y., Chen, B. (2000). Massive granitoid generation in central Asia: Nd
572 isotopic evidence and implication for continental growth in the Phanerozoic. Episodes,
573 23, 82-92.
574 Jiang, H. (2016). Granite magmatism and tectonic setting of "Five Golden Flower" granite

plutons in Lixian-Minxian ore concentrated area, Western Qinling. Northwest University, master's thesis.

Jiang, Y. H., Jin, G. D., Liao, S. Y., Zhou, Q., Zhao, P. (2010). Geochemical and Sr-Nd-Hf isotopic constraints on the origin of late Triassic granitoids from the qinling orogen, central china: implications for a continental arc to continent-continent collision. Lithos, 117(1-4), 183-197.

King, P. L., White, A. J. R., Chappell, B. W., Allen, C. M. (1997). Characterization and origin of aluminous a-type granites from the lachlan fold belt, southeastern australia. Journal of Petrology, 38(3), 371-391.

Kong, J.J., Niu, Y.L., Duan, M., Zhang, Y., Hu, Y., Li, J.Y., Chen, S. (2017). Petrogenesis of Luchuba and Wuchaba granitoids in western Qinling: geochronological and geochemical evidence. Mineralogy and Petrology, 111, 887-908.

Lai, S.C., Zhang, G.W. (1996). Geochemical features of ophiolites in Mianxian–Lueyang suture zone, Qinling Orogenic Belt. Journal of China University of Geosciences, 7, 165-172.

Leake, B. E., Woolley, A. R., Arps, C. E. S., Birch, W. D., Gilbert, M. C., Grice, J. D. (1997). Nomenclature of amphiboles; Report of the Subcommittee on Amphiboles of the International Mineralogical Association, Commission on New Minerals and Mineral Names. International Conference on Formal Concept Analysis, 4390, 181-196.

Lee, C. T. A., Anderson, D. L. (2015). Continental crust formation at arcs, the arclogite "delamination" cycle, and one origin for fertile melting anomalies in the mantle. Science Bulletin, 60 (13), 1141-1156.

597 Li, X. H., Liu, D., Sun, M. I. N., Li, W. X., Liang, X. R., Liu, Y. (2004). Precise Sm-Nd and
598 U-Pb isotopic dating of the supergiant Shizhuyuan polymetallic deposit and its host
599 granite, SE China. Geological Magazine, 141(02), 225-231.
600 Li, X.H., Li, Z.X., Li, W.X., Liu, Y., Yuan, C., Wei, G.J., Qi, C.S. (2007). U-Pb zircon,
601 geochemical and Sr-Nd-Hf isotopic constraints on age and origin of Jurassic I- and A-
602 type granites from central Guangdong, SE China: a major igneous event in response to
603 foundering of a subducted flat-slab? Lithos, 96, 186-204.
604
605 Li, Y., Liang, W., Zhang, G., Jiang, D., Wang, J. (2017). Tectonic setting of the late triassic
606 magmatism in the qinling orogen: new constraints from the interplay between granite
607 emplacement and shear zone deformation in the shagou area. Geological Journal, 52(S1).
608 Liang, W., Zhang, G., Bai, Y., Jin, C., Nantasin, P. (2015). New insights into the
609 emplacement mechanism of the late Triassic granite plutons in the Qinling orogen: a
610 structural study of the mishuling pluton. Geological Society of America Bulletin, 127,
611 11-12.
612 Lin, W.W., Peng, L.J. (1994). The estimation of Fe^{3+} and Fe^{2+} contents in amphibole and
613 biotite from EMPA data. Journal of Changchun University Earth Sciences, 24, 155-162
614 (in Chinese with English abstract).
615 Li, Y. J., Duan, Y. M., Li, X. F. (1993). Tnternal contact relationship and geological mapping
616 of super unit and unit system for granites in the Taoping Region of the western Qinling
617 [J]. Journal of Xi′an College of Geology, 15, 98-106.
618 Liu, F.L., Xu, Z.Q., Liou, J.G., Song, B. (2004). SHRIMP U-Pb ages of ultrahigh-pressure

and retrograde metamorphism of gneisses, south-western Sulu terrane, eastern China. Journal of Metamorphic Geology, 22, 315-326.

Liu, S.W., Li, Q.G., Tian, W., Wang, Z.Q., Yang, P.T., Wang, W., Bai, X., Guo, R.R. (2011a). Petrogenesis of Indosinian granitoids in Middle-Segment of South Qinling Tectonic Belt: constraints from Sr-Nd isotopic systematics. Acta Geologica Sinica-English edition, 85, 610-628.

Liu, S.W., Yang, P.T., Li, Q.G., Wang, Z.Q., Zhang, W.Y., Wang, W. (2011b). Indosinian Granitoids and orogenic processes in the middle segment of the Qinling orogen, China. Journal of Jilin university (Earth science Edition), 41(6).

Ludwig, K. (2012). User's manual for Isoplot version 3.75-4.15: a geochronological toolkit for Microsoft. Excel Berkley Geochronological Center Special Publication, No. 5.

Mattauer, M., Matte, P., Malavieille, J., Tapponnier, P., Maluski, H., Qin, X. Z., Qin, T. Y. (1985). Tectonics of the Qinling belt: Build-up and evolution of eastern Asia. Nature, 317, 496-500.

Meng, Q.R., Zhang, G.W. (2000). Geologic framework and tectonic evolution of the Qinling-Dabie orogen, central China. Tectonophysics, 323, 183-196.

Mo, X. X., Niu, Y. L., Dong, G. C., Zhao, Z. D., Hou, Z. Q., Zhou, S., Ke, S. (2008). Contribution of syncollisional felsic magmatism to continental crust growth: a case study of the Paleogene Linzizong volcanic succession in southern Tibet. Chemical Geology, 250, 49-67.

Ni, Z.Y., Chen, Y.J., Li, N., Zhang, H. (2012). Pb-Sr-Nd isotope constraints on the fluid source of the Dahu Au-Mo deposit in Qinling Orogen, central China, and implication

641 for Triassic tectonic setting. Ore Geology Reviews, 46(8), 60-67.
642 Niu, Y.L. (2017). Slab breakoff: A causal mechanism or pure convenience? Science Bulletin,
643 62, 456-461.
644 Niu, Y.L., Mo, X.X., Dong, G.C., Zhao, Z.D., Hou, Z.Q., Zhou, S., Ke, S. (2007). Continental
645 collision zones are primary sites of net continental crustal growth: Evidence from the
646 Linzizong volcanic succession in southern Tibet. Eos Trans. AGU, 88(52), Fall Meet.,
647 Suppl., Abstract 34, 01.
648 Niu, Y. L., O'Hara, M. J. (2009). MORB mantle hosts the missing Eu (Sr, Nb, Ta and Ti) in
649 the continental crust: New perspectives on crustal growth, crust-mantle differentiation
650 and chemical structure of oceanic upper mantle. Lithos, 112, 1-17.
651 Niu, Y. L., Zhao, Z. D., Zhu, D. C., Mo, X. X. (2013). Continental collision zones are primary
652 sites for net continental crust growth-A testable hypothesis. Earth Science Reviews, 127,
653 96-110.
654 Qin, J.F., Lai, S.C., Grapes, R., Diwu, C.R., Ju, Y.J., Li, Y.F. (2009). Geochemical evidence
655 for origin of magma mixing for the Triassic monzonitic granite and its enclaves at
656 Mishuling in the Qinling orogen (central China). Lithos, 112, 259-276.
657 Qin, J.F., Lai, S.C., Grapes, R., Diwu, C.R., Ju, Y.J., Li, Y.F. (2010). Origin of Late Triassic
658 high Mg adakitic granitoid rocks from the Dongjiangkou area, Qinling orogen, central
659 China implications for subduction of continental crust. Lithos, 120, 347-367.
660 Pearce, J.A., Peate, D.W. (1995). Tectonic implications of the composition of volcanic arc
661 magmas. Annual Review of Earth and Planetary Sciences, 23, 251-286.
662 Peng, X. (2013). Research on homology for the rock group of monzonite granite in the

western qinling. Northwestern Geology, 46, 63-80.

Pin, C., Binon, M., Belin, J. M., Barbarin, B., Clemens, J. D. (1990). Origin of microgranular enclaves in granitoids: equivocal Sr-Nd evidence from hercynian rocks in the massif central (france). Journal of Geophysical Research Solid Earth, 95(B11), 17821-17828.

Poli, G. E., Tommasini, S. (1991). Model for the origin and significance of microgranular enclaves in calc-alkaline granitoids. Journal of Petrology, 32(3), 657-666.

Ratschbacher, L., Hacker, B.R., Calvert, A., Webb, L.E., Crimmer, J.C., McWilliams, M.O., Ireland, T., Dong, S., Hu, J. (2003). Tectonics of the Qinling (Central China): tectonostratigraphy, geochronology, and deformation history. Tectonophysics, 366, 1-53.

Jr, J. B. R., Hamilton, M. A. (1987). Origin of sierra nevadan granite: evidence from smallscale composite dikes. Contributions to Mineralogy and Petrology, 96(4), 441-454.

Reiners, P. W., Nelson, B. K., Ghiorso, M. S. (1995). Assimilation of felsic crust by basaltic magma: thermal limits and extents of crustal contamination of mantle-derived magmas. Geology, 23(6), 563.

Reiners, P. W., Nelson, B. K., Nelson, S. W. (1996). Evidence for multiple mechanisms of crustal contamination of magma from compositionally zoned plutons and associated ultramafic intrusions of the Alaska Range. Journal of Petrology, 37(2), 261-292.

Rollison, H. (1993). Using geochemical data: Evaluation, presentation, interpretation. London, Longman Scientific and Technical, 352.

Rubatto, D., Gebauer, D. (2000). Use of cathodoluminescence for U-Pb zircon dating by ion microprobe: some examples from the Western Alps. Cathodoluminescence in

685 Geosciences, Springer, Berlin, 373-400.

686 Rudnick, R. L., Gao, S. (2003). Composition of the continental crust. Treatise on
687 Geochemistry, 3, 1-64.

688 Shao, F. L., Niu, Y. L., Liu, Y., Chen, S., Kong, J.J., Duan, M. (2017). Petrogenesis of triassic
689 granitoids in the east kunlun orogenic belt, northern tibetan plateau and their tectonic
690 implications. Lithos, 282-283, 33-44.

691 Shen, J., Zhang, Z. Q., Liu, D. Y. (1997). Sm-Nd, Rb-Sr, $^{40}Ar/^{39}Ar$, $^{207}Pb/^{206}Pb$ age of the
692 Douling metamorphic complex from eastern Qinling orogenic belt. Acta Geoscientia
693 Sinica 18(3), 248-254.

694 Song, S., Niu, Y., Wei, C., Ji, J., Su, L. (2010a). Metamorphism, anatexis, zircon ages and
695 tectonic evolution of the Gongshan block in the northern Indochina continent-an eastern
696 extension of the Lhasa Block. Lithos,120 (3), 327-346.

697 Song, S. G., Su, L., Li, X. H., Zhang, G. B., Niu, Y. L., Zhang, L. F. (2010b). Tracing the
698 850-Ma continental flood basalts from a piece of subducted continental crust in the
699 North Qaidam UHPM belt, NW China. Precambrian Research, 183, 805-816.

700 Sun et al., 2018. Multiple mantle metasomatism beneath the Leizhou Peninsula, South China:
701 Evidence from elemental and Sr-Nd-Pb-Hf isotope geochemistry of the late Cenozoic
702 volcanic rocks (in prepration).

703 Sun, W.D., Li, S.G., Chen, Y.D., Li, Y.J. (2002). Timing of synorogenic granitoids in the
704 South Qinling, central China: constraints on the evolution of the Qinling-Dabie orogenic
705 belt. Journal of Geology, 110, 457-468.

706 Sun, S.s., McDonough, W. F. (1989). Chemical and isotopic systematics of oceanic basalts:

707 implications for mantle composition and processes. Geological Society, London,
708 Special Publications, 42, 313-345.
709 Taylor, S. R. (1967). The origin and growth of continents. Tectonophysics, 4, 17-34.
710 Vervoort, J.D., Patchett, P.J., Blichert-Toft, J., Albarède, F. (1999). Relationships between
711 Lu-Hf and Sm-Nd isotopic systems in the global sedimentary system. Earth and
712 Planetary Science Letters, 168, 79-99.
713 Vervoort, J.D., Plank, T., Prytulak, J. (2011). The Hf-Nd isotopic composition of marine
714 sediments. Geochimica et Cosmochimica Acta, 75, 5903-5926.
715 Wang, Z.Q., Yan, Q. R., Yan, Z., Wang, T., Jiang, C.F., Gao, L.D., Liu, P. (2009). The new
716 division of the main tectonic unit for the Qinling orogenic belt. Journal of Geology,
717 3(11), 1527-1546.
718 Wen, Z.L. (2008). A new recognition of magma mixing process about jiaochangba rock body,
719 western qinling. Journal of Mineralogy and Petrology, 3, 29-36.
720 Whalen, J.B. (1985). Geochemistry of an island-arc plutonic suite: the Uasilau-Yau Yau
721 intrusive complex, New Britain P.N.G: Journal of Petrology, 26, 603-632.
722 Whalen, J.B., Currie, K.L., Chappell, B.W. (1987). A-type granites: Geochemical
723 characteristics, discrimination and petrogenesis. Contributions to Mineralogy and
724 Petrology, 95, 407-419.
725 Wiedenbeck, M., Alle, P., Corfu, F., Griffin, W.L., Meier, M., Oberli, F., Vonquadt, A.,
726 Roddick, J.C., Speigel, W. (1995). Three natural zircon standards for U-Th-Pb, Lu-Hf,
727 trace-element and REE analyses. Geostandard Newsletter, 19, 1-23.
728 Wu, Y.B., Zheng, Y.F. (2012). Tectonic evolution of a composite collision orogen: an

overview on the Qinling-Tongbai-Hong'an-Dabie-Sulu orogenic belt in central China. Gondwana Research, 23, 1402-1428.

Xiao, B., Li, Q., Liu, S., Wang, Z., Yang, P., Chen, J., Xu, X. (2014). Highly fractionated Late Triassic I-type granites and related molybdenum mineralization in the Qinling orogenic belt: Geochemical and U-Pb-Hf and Re-Os isotope constraints. Ore Geology Reviews, 56, 220-233.

Xiao, L. (2004). Geological map of Minxian and Tianshui: Chinese Geological Survey, scale 1: 250,000, 2 sheets.

Xu, J.F., Castillo, P. R., Li, X.H., Zhang, B.R., Han, Y.W. (2002). MORB-type rocks from the Paleo-Tethyan mian-lueyang northern ophiolite in the Qinling mountains, central china: Implications for the source of the low $^{206}Pb/^{204}Pb$ and high $^{143}Nd/^{144}Nd$ mantle component in the Indian ocean. Earth and Planetary Science Letters, 198, 323-337.

Xu, Y.L., M, Y. Z., Wang, G.G. (2006). Discusson diagenetic and metallogenic features and metallogenic Mechanism of Bojiazhuang rock mass in Minxian-Lixian area of Gansu province. Gansu Geology, 15, 126-132.

Yuan, H. L., Fuyuan, W. U., Shan, G., Liu, X., Ping, X. U., Sun, D. (2003). Determination of U-Pb age and rare earth element concentrations of zircons from cenozoic intrusions in northeastern china by laser ablation ICP-MS. Science Bulletin, 48, 2411-2421.

Yan, Z., Wang, Z., Li, J., Xu, Z., Deng, J. (2012). Tectonic settings and accretionary orogenesis of the West Qinling Terrane, northeastern margin of the Tibet Plateau. Acta Petrologica Sinica, 28, 1808-1828.

Yang, J.S., Wu, F.Y., Wilde, S., Liu, X. (2007). Petrogenesis of late Triassic granitoids and

751 their enclaves with implications for post-collisional lithospheric thinning of the
752 Liaodong Peninsula, North China Craton. Chemical Geology, 242, 155-175.
753 Yang, P.T., Liu, S.W., Li, Q.G., Zhang, F., Wang, Z.Q., Wang, D.S., Wang, R.T., Yan, Q.R.,
754 Yan, Z. (2011). Ages of the Laocheng granitoids and crustal growth in the South Qinling
755 Tectonic Domain, Central China: zircon U-Pb and Lu-Hf isotopic constraints. Acta
756 Geologica Sinica-English edition, 85, 854-869.
757 Yang, P.T., Liu, S.W., Li, Q.G., Wang, Z.Q., Wang, R.T., Wang, W. (2012). Geochemistry and
758 zircon U-Pb-Hf isotopic systematics of the Ningshan granitoid batholith, middle
759 segment of the South Qinling belt, Central China: constraints on petrogenesis and
760 geodynamic processes. Journal of Asian Earth Sciences, 61, 166-186.
761 Yang, S. S., Liu, J. J., Zhang, F., Yuan, F., Zhai, D. G., Li, Y. J. (2017). Petrogenesis and
762 geodynamic setting of the Triassic granitoid plutons in West Qinling, China: insights
763 from LA-ICP-MS zircon U-Pb ages, Lu-Hf isotope signatures and geochemical
764 characteristics of the zhongchuan pluton. Intenational Geology Review, 2, 1-21.
765 Yang, Y., Wang, X.X., Ke, C.H., Wang, S.A., Li, J.B., Nie, Z.R., LV, X.Q. (2015). Zircon U-
766 Pb Ages and Petrogenesis of the Luchuba Pluton in West Qinling, and Its Geological
767 Significance. Acta Geologica Sinica, 89, 1735-1761.
768 Yang, Y. H., Zhang, H. F., Chu, Z. Y., Xie, L. W., Wu, F. Y. (2010). Combined chemical
769 separation of Lu, Hf, Rb, Sr, Sm and Nd from a single rock digest and precise and
770 accurate isotope determinations of Lu-Hf, Rb-Sr and Sm-Nd isotope systems using
771 Multi-Collector ICP-MS and TIMS. International Journal of Mass Spectrometry, 290,
772 120-126.

773 Zhang, C.L., Zhang, G.W., Yan, Y.X., Wang, Y. (2005). Origin and dynamic significance of
774 Guangtoushan granitic plutons to the north of Mianlue zone in southern Qinling. Acta
775 Petrologica Sinca, 21, 711-720.
776 Zhang, G.W., Zhang, B.R., Yuan, X.C., Xiao, Q.H. (2001). Qinling Orogen Belt and
777 Continental Geodynamics. Science Press: Beijing, 1-729.
778 Zhang, H., Jin, L., Zhang, L., Nigel, H., Zhou, L., Hu, S., Zhang, B. (2007). Geochemical
779 and Pb-Sr-Nd isotopic compositions of granitoids from western Qinling belt:
780 Constraints on basement nature and tectonic affinity. Science in China Series D: Earth
781 Sciences, 50, 184-196.
782 Zhang, Y., Y.L. Niu, Y. Hu, J.J. Liu, L. Ye, J.J. Kong., M. Duan. (2016). The syncollisional
783 granitoid magmatism and continental crustal growth in the West Kunlun Orogen, China
784 -Evidence from geochronology and geochemistry of the Arkarz pluton. Lithos, 245,
785 191-204.
786 Zhang, Z.Q., Zhang, G.W., Tang, S.H. (2002). Isotopic Chronology of South Qinling
787 Metamorphic Rock-Group. Beijing, Geological Publishing House, 1-256.
788 Zheng, Y.F. (2008). A perspective view on ultrahigh-pressure metamorphism and continental
789 collision in the Dabie-Sulu orogenic belt. Chinese Science Bulletin, 53, 3081-3104.
790 Zhong, H., Zhu, W.G., Hu, R.Z., Xie, L.W., He, D.F., Liu, F., Chu, Z.Y. (2009). Zircon U-
791 Pb age and Sr-Nd-Hf isotope geochemistry of the Panzhihua A-type syenitic intrusion
792 in the Emeishan large igneous province, southwest China and implications for growth
793 of juvenile crust. Lithos, 110, 109-128.
794 Zhu, L. M., Zhang, G. W., Chen, Y. J., Ding, Z. J., Guo, B., Wang, F., Lee, B. (2011). Zircon

U-Pb ages and geochemistry of the Wenquan Mo-bearing granitioids in West Qinling, China: Constraints on the geodynamic setting for the newly discovered Wenquan Mo deposit. Ore Geology Reviews, 39, 46-62.

Zhu, L., Zhang, G., Yang, T., Wang, F., Gong, H. (2013). Geochronology, petrogenesis and tectonic implications of the Zhongchuan granitic pluton in the Western Qinling metallogenic belt, China. Geological Journal, 48, 310-334.

Figure captions

Figure 1. ***(a)***, ***(b)*** Simplified geological map of the Western Qinling Orogenic belt (modified from Zhang et al., 2007). ***(c)*** Modified from 1:250,000 geological map of Minxian and Tianshui sheets (Xiao, 2004). The abbreviations are as follows: JCB = Jiaochangba, LCB = Luchuba, WCB = Wuchaba, LJ = Lvjing, BJZ = Baijiazhuang.

Figure 2. ***(a)***, ***(b)*** An outcrop of JCB granitoid pluton with mafic magmatic enclaves (MMEs). ***(c)*** Photomicrographs of the JCB granitoid host (cross-polarized light or XPL) ***(d)*** Photomicrographs of the JCB MME (XPL). Showing the same mineralogy between the host granodiorite and their MMEs and the MMEs have greater mafic mineral modes. The abbreviations are as follows: Pl - Plagioclase, Qz - Quartz, Bt - Biotite, Hb - Hornblende.

Figure 3. Zircon U-Pb concordia plots and weighted mean $^{206}Pb/^{238}U$ ages for ***(a)*** JCB12-07 and ***(b)*** JCB12-12 of the JCB pluton.

Figure 4. Plagioclase composition in granitoid hosts (JCB12-10) and the MME (JCB12-11).

816 See Table 3a for compositional data.

817 **Figure 5.** Chemical compositions of amphiboles from granitoid hosts (JCB12-10) and the
818 MME (JCB12-11) in the amphibole classification diagram (Leake et al., 1997). See Table 3a
819 for compositional data.

820 **Figure 6**. ***(a)*** Total alkalis (Na_2O + K_2O) versus SiO_2 (TAS) diagram showing the
821 compositional variation of the JCB samples. The MME is less felsic than the granitic hosts.
822 ***(b)*** Diagram of K_2O vs. SiO_2 for granitoids of JCB pluton. ***(c)*** Diagram of A/NK [Al_2O_3/
823 (Na_2O + K_2O)] vs. A/CNK [molar ratio Al_2O_3/ (CaO + Na_2O + K_2O)] for granitoids of JCB
824 pluton.

825 **Figure 7**. SiO_2 variation diagrams of representative major element oxides (wt.%) and
826 selected trace elements (ppm) of the JCB samples.

827 **Figure 8**. ***(a)*** Chondrite normalized REE patterns, and ***(b)*** N-MORB normalized
828 incompatible element abundances of samples from the JCB pluton; For comparison, the
829 average Bulk continental crust (BCC, red solid line) (Rudnick and Gao, 2003) is also plotted.
830 Chondrite and N-MORB values are from Sun and McDonough (1989). The data of shades of
831 grey are from Duan et al. (2016); Kong et al. (2017).

832 **Figure 9**. ***(a)-(c)*** Plots of Sr, Nd and Hf isotopes (in the forms of initial $^{87}Sr/^{86}Sr$ or I_{Sr}, $\varepsilon_{Nd}(t)$
833 and $\varepsilon_{Hf}(t)$) against SiO_2, showing isotopes between MMEs with lower SiO_2 and the host
834 granitoids with higher SiO_2. The data of LJ, BJZ from Duan et al. (2016) and the data of
835 WCB, LCB from Kong et al. (2017). ***(d)*** The $\varepsilon_{Nd}(t)$ of upper crust (mature crust) is from

836 Reiners et al. (1995) and the $\varepsilon_{Hf}(t)$ is inferred from Nd isotope following the equation (ε_{Hf} =
837 $1.59\varepsilon_{Nd} + 1.28$) given by (Chauvel et al., 2008). The field for crust-mantle array is from
838 Vervoort et al. (1999) and the terrestrial array is from Vervoort et al. (2011).

839 **Figure10**. ***(a)*** CaO versus Eu/Eu* diagram; ***(b)*** CaO versus Sr diagram. The graphic symbol
840 as Figure 5.

841 **Figure11**. ***(a)*** Sr versus Ba diagram; ***(b)*** Sr versus Rb diagram.

842 **Figure 12**. Plot of $^{87}Sr/^{86}Sr$ vs. $\varepsilon_{Nd}(t)$ for JCB granitoids. The modeled AFC path uses parental
843 magma (Mianlue MORB) with 93 ppm Sr (I_{Sr}: 0.705), 6.5 ppm Nd ($\varepsilon_{Nd}(t)$: 8.71) (Xu et al.,
844 2002) and a hypothetical basement rock Douling gneiss from south Qinling with 268 ppm Sr
845 (I_{Sr}: 0.721) and 26 ppm Nd ($\varepsilon_{Nd}(t)$: -14.5) (Shen et al., 1997) for conceptual simplicity. AFC
846 path calculated according to (DePaolo et al., 1981) equation. The ratio of assimilation to
847 fractionation was set at r = 0.15. Bulk Kd's for Sr and Nd were 0.36 and 0.86, respectively.

848 **Figure 13**. Schematic illustration for the generation of the JCB granitoids in West Qinling
849 during the late Triassic (~220Ma). See text for explanation.

850 **Table captions**

851 **Table 1.** Summary of lithologies, geochemistry, and geochronology of the five granitoid
852 plutons in the West Qinling.

853 **Table 2.** Zircon U-Pb data for the Jiaochangba pluton.

854 **Table 3.** a. Microprobe analysis of plagioclase in the host granitoids and the mafic magmatic
855 enclaves; b. Microprobe analysis of amphibole in the host granitoids and the mafic magmatic
856 enclaves.

857 **Table 4.** Major (wt.%) and trace element concentrations (ppm) of the Jiaochangba pluton.

858 **Table 5.** Sr, Nd, Hf isotopes of the Jiaochangba pluton.

859 **Appendix A.** The Sr-Nd-Hf isotopes replicate analyses results of the international reference
860 materials.

Fig.1

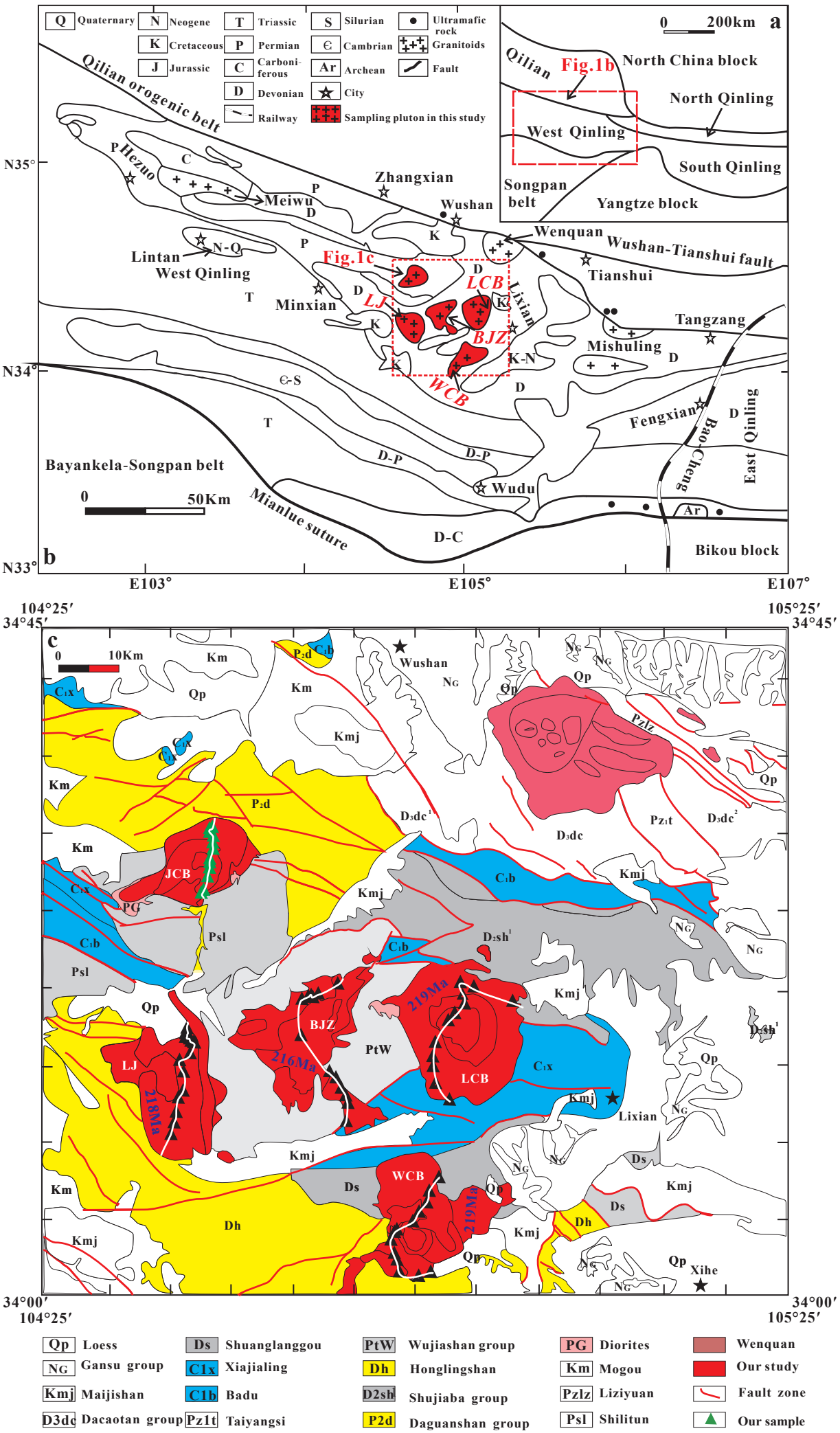
Q Quaternary
N Neogene
K Cretaceous
J Jurassic
T Triassic
P Permian
C Carboni-ferous
D Devonian
Railway
S Silurian
Ar Archean
City
Sampling pluton in this study
Ultramafic rock
Granitoids
Fault
0 200km
a
Qilian
Fig.1b
North China block
North Qinling
West Qinling
South Qinling
Songpan belt
Yangtze block
Qilian orogenic belt
Hezuo
Meiwu
Zhangxian
Wushan
Wenquan
Wushan-Tianshui fault
Lintan
West Qinling
Fig.1c
Minxian
LCB
LJ
BJZ
WCB
Lixian
Tianshui
Tangzang
Mishuling
Fengxian
Bao-Chen
East Qinling
Bayankela-Songpan belt
Wudu
Mianlue suture
Bikou block
0 50Km
b
N35°
N34°
N33°
E103°
E105°
E107°
104°25′
34°45′
105°25′
c
0 10Km
Wushan
Qp
Km
Kmj
Pzlz
Pzt
D3dc
JCB
PG
Psl
C1b
C1x
D2sh
219Ma
216Ma
218Ma
PtW
LJ
BJZ
LCB
WCB
Lixian
Xihe
Ds
Dh
NG
34°00′
104°25′
105°25′
Qp Loess
NG Gansu group
Kmj Maijishan
D3dc Dacaotan group
Ds Shuanglanggou
C1x Xiajialing
C1b Badu
Pz1t Taiyangsi
PtW Wujiashan group
Dh Honglingshan
D2sh Shujiaba group
P2d Daguanshan group
PG Diorites
Km Mogou
Pzlz Liziyuan
Psl Shilitun
Wenquan
Our study
Fault zone
Our sample

Fig.2

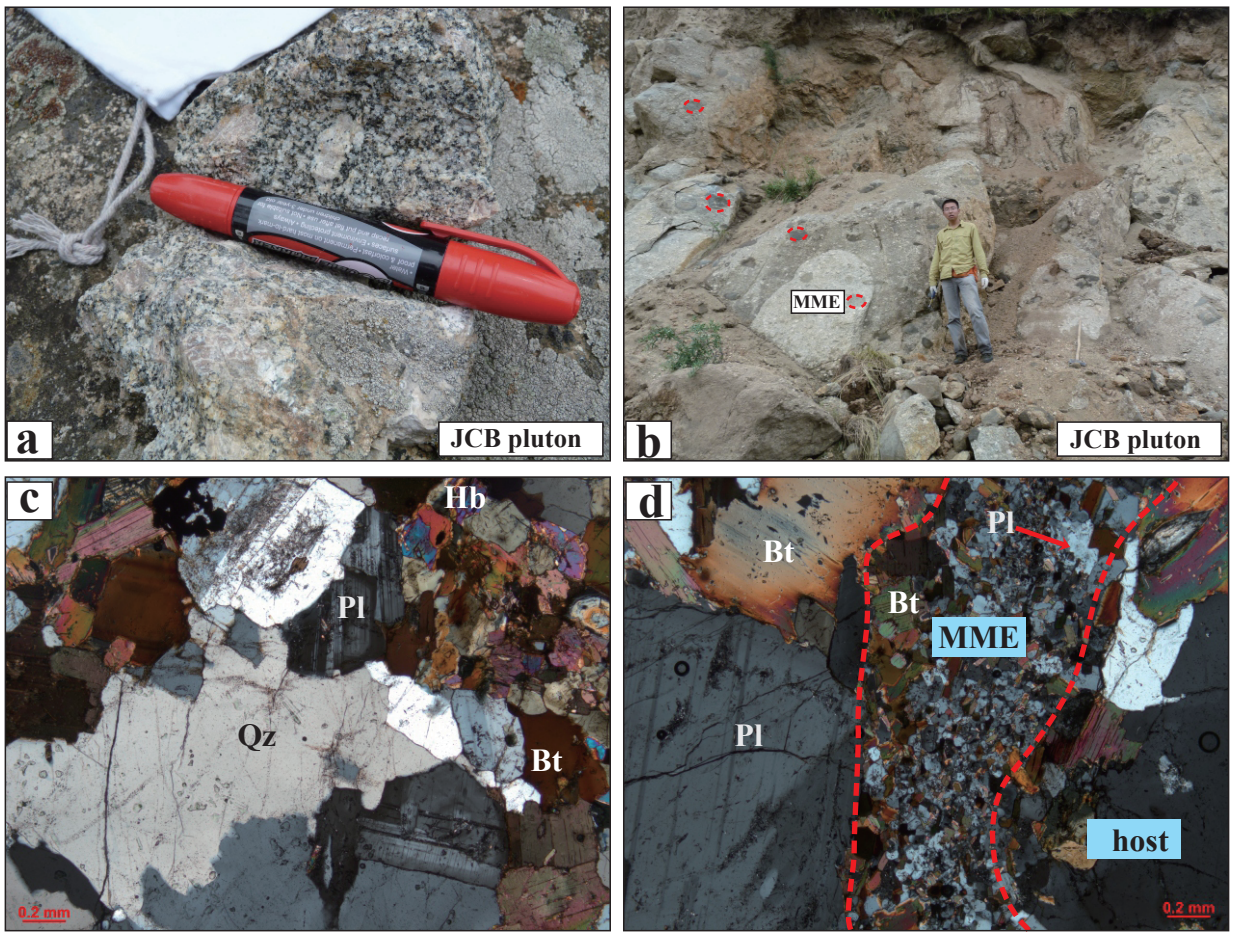
a
JCB pluton
b
MME
JCB pluton
c
Hb
Pl
Qz
Bt
0.2 mm
d
Bt
Pl
Bt
MME
Pl
host
0.2 mm

Fig.3

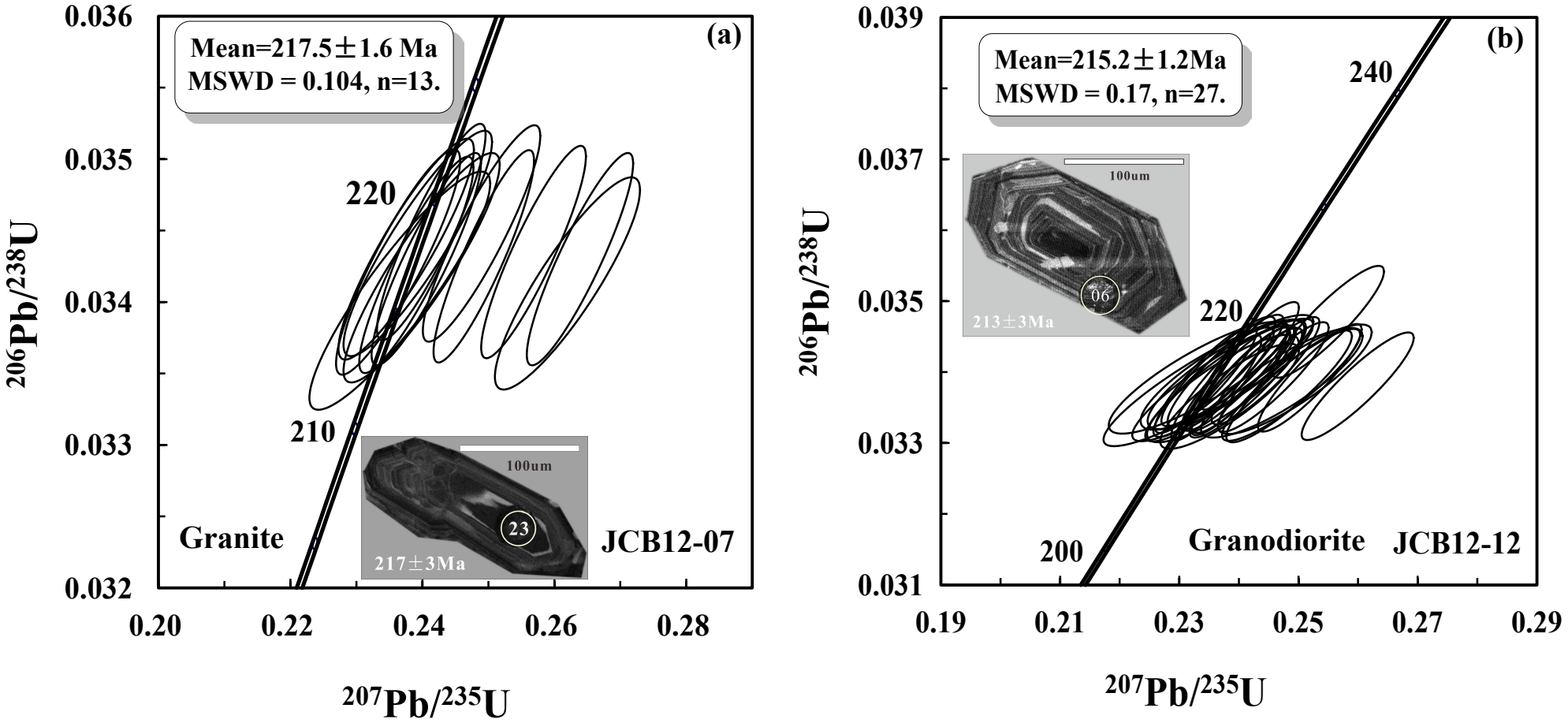
(a)
Mean=217.5±1.6 Ma
MSWD = 0.104, n=13.
220
210
Granite
JCB12-07
100um
23
217±3Ma
0.036
0.035
0.034
0.033
0.032
0.20
0.22
0.24
0.26
0.28
206Pb/238U
207Pb/235U
(b)
Mean=215.2±1.2Ma
MSWD = 0.17, n=27.
240
220
200
Granodiorite
JCB12-12
100um
06
213±3Ma
0.039
0.037
0.035
0.033
0.031
0.19
0.21
0.23
0.25
0.27
0.29
206Pb/238U
207Pb/235U

Fig.4

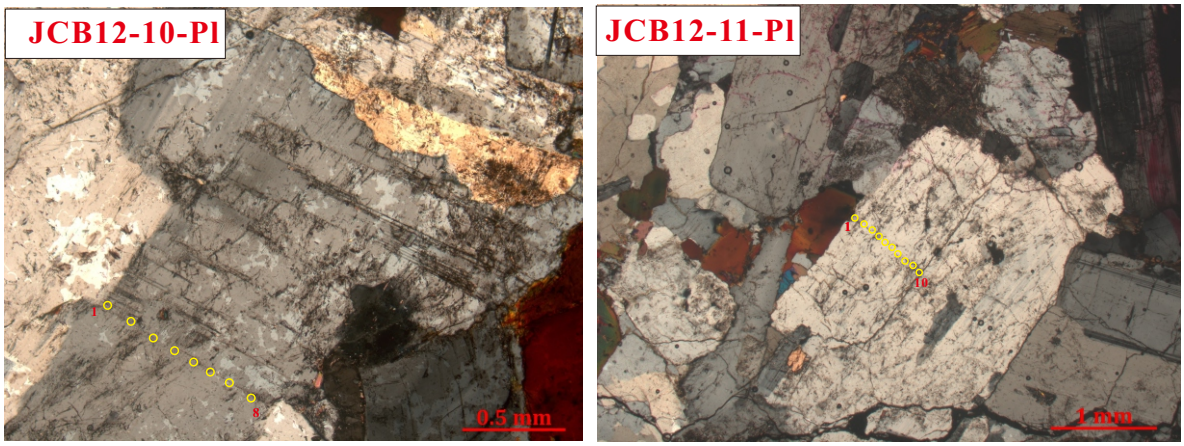

Fig.5

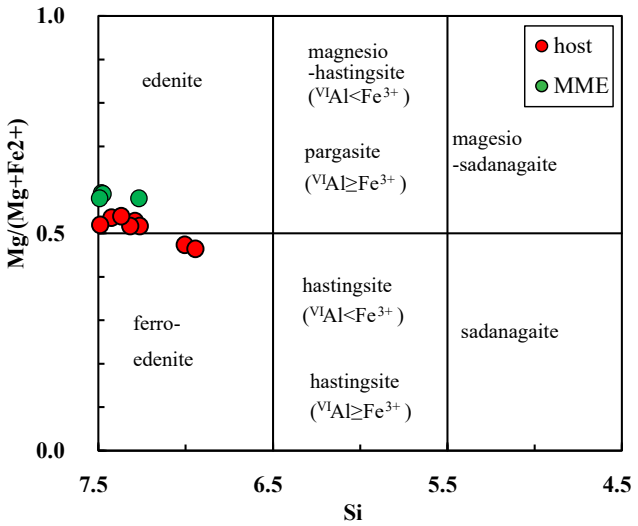
1.0
0.5
0.0
Mg/(Mg+Fe2+)
7.5
6.5
5.5
4.5
Si
edenite
magnesio
-hastingsite
(VIAl<Fe3+)
pargasite
(VIAl≥Fe3+)
magesio
-sadanagaite
ferro-
edenite
hastingsite
(VIAl<Fe3+)
hastingsite
(VIAl≥Fe3+)
sadanagaite
host
MME

Fig.6

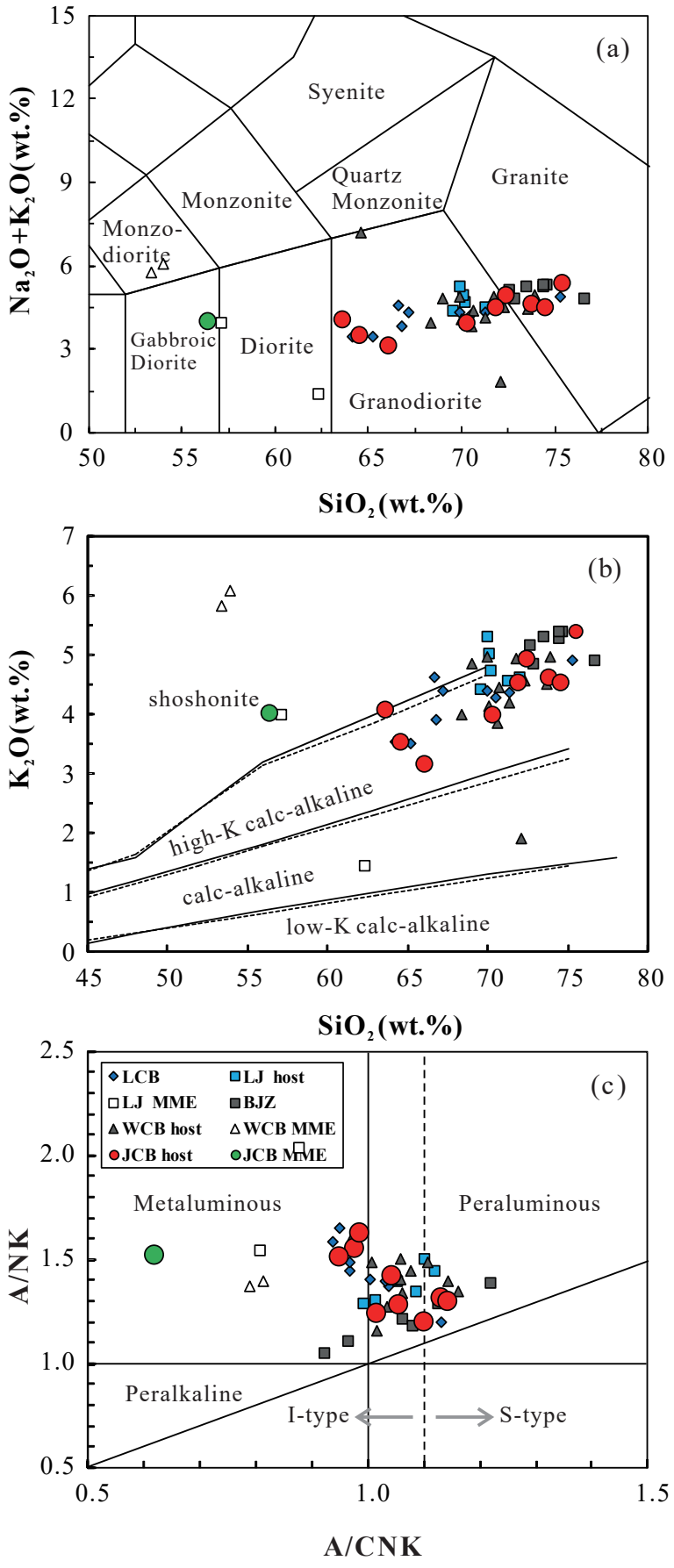
(a)
Syenite
Quartz Monzonite
Granite
Monzonite
Monzo-diorite
Gabbroic Diorite
Diorite
Granodiorite
Na_2O+K_2O(wt.%)
SiO_2(wt.%)
(b)
shoshonite
high-K calc-alkaline
calc-alkaline
low-K calc-alkaline
K_2O(wt.%)
SiO_2(wt.%)
(c)
LCB
LJ host
LJ MME
BJZ
WCB host
WCB MME
JCB host
JCB MME
Metaluminous
Peraluminous
Peralkaline
I-type
S-type
A/NK
A/CNK

Fig.7

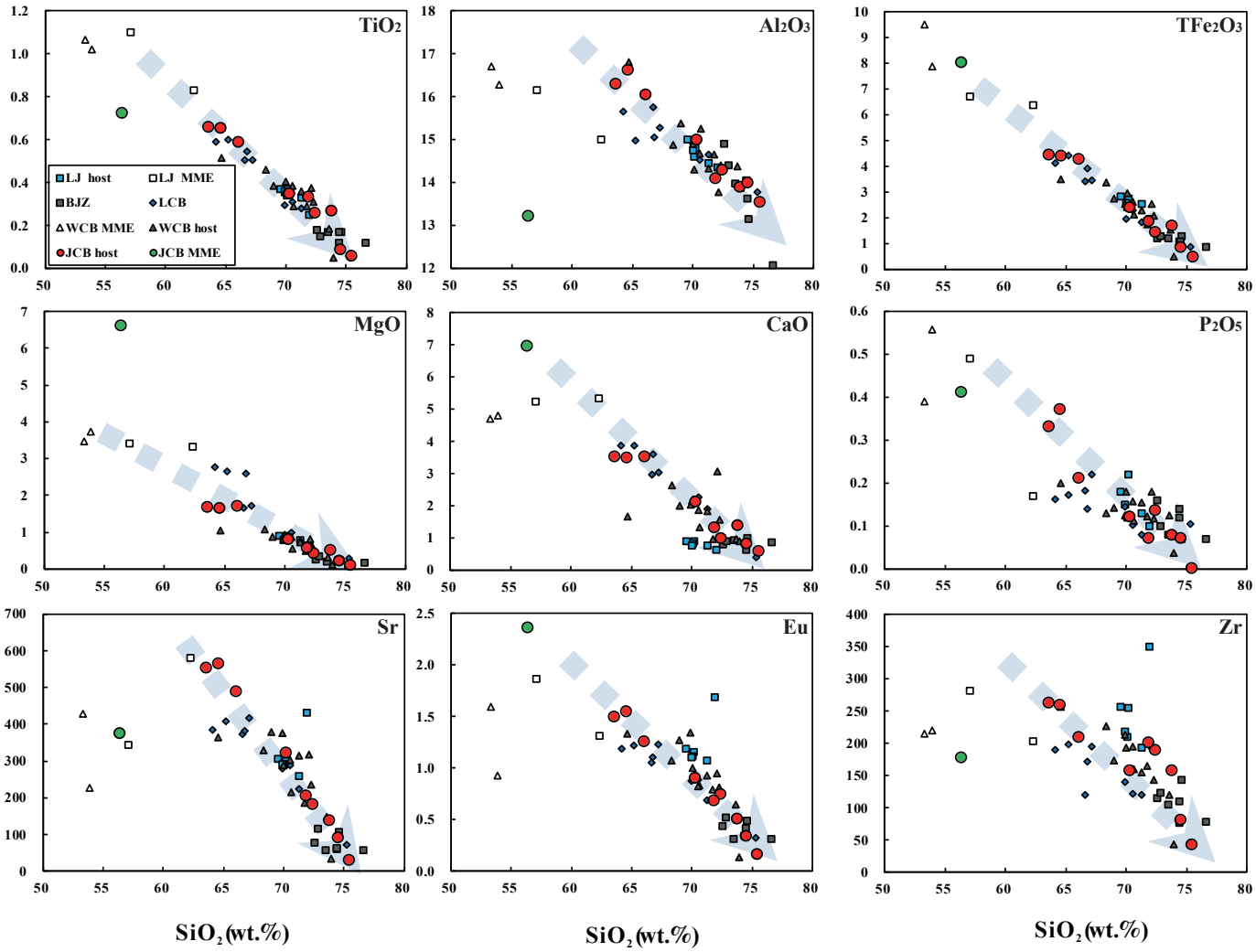
TiO2
Al2O3
TFe2O3
MgO
CaO
P2O5
Sr
Eu
Zr
LJ host
LJ MME
BJZ
LCB
WCB MME
WCB host
JCB host
JCB MME
SiO2(wt.%)
SiO2(wt.%)
SiO2(wt.%)

Fig.8

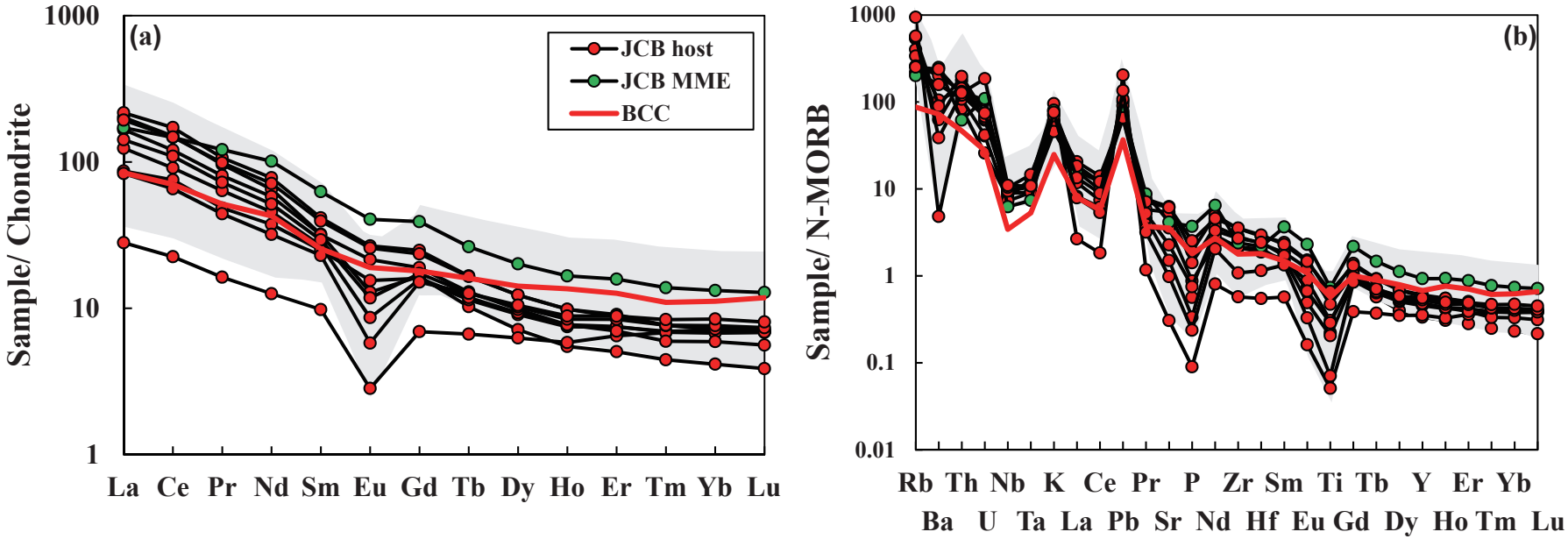
(a)
JCB host
JCB MME
BCC
Sample/ Chondrite
1000
100
10
1
La Ce Pr Nd Sm Eu Gd Tb Dy Ho Er Tm Yb Lu
(b)
Sample/ N-MORB
1000
100
10
1
0.1
0.01
Rb Th Nb K Ce Pr P Zr Sm Ti Tb Y Er Yb
Ba U Ta La Pb Sr Nd Hf Eu Gd Dy Ho Tm Lu

Fig.9

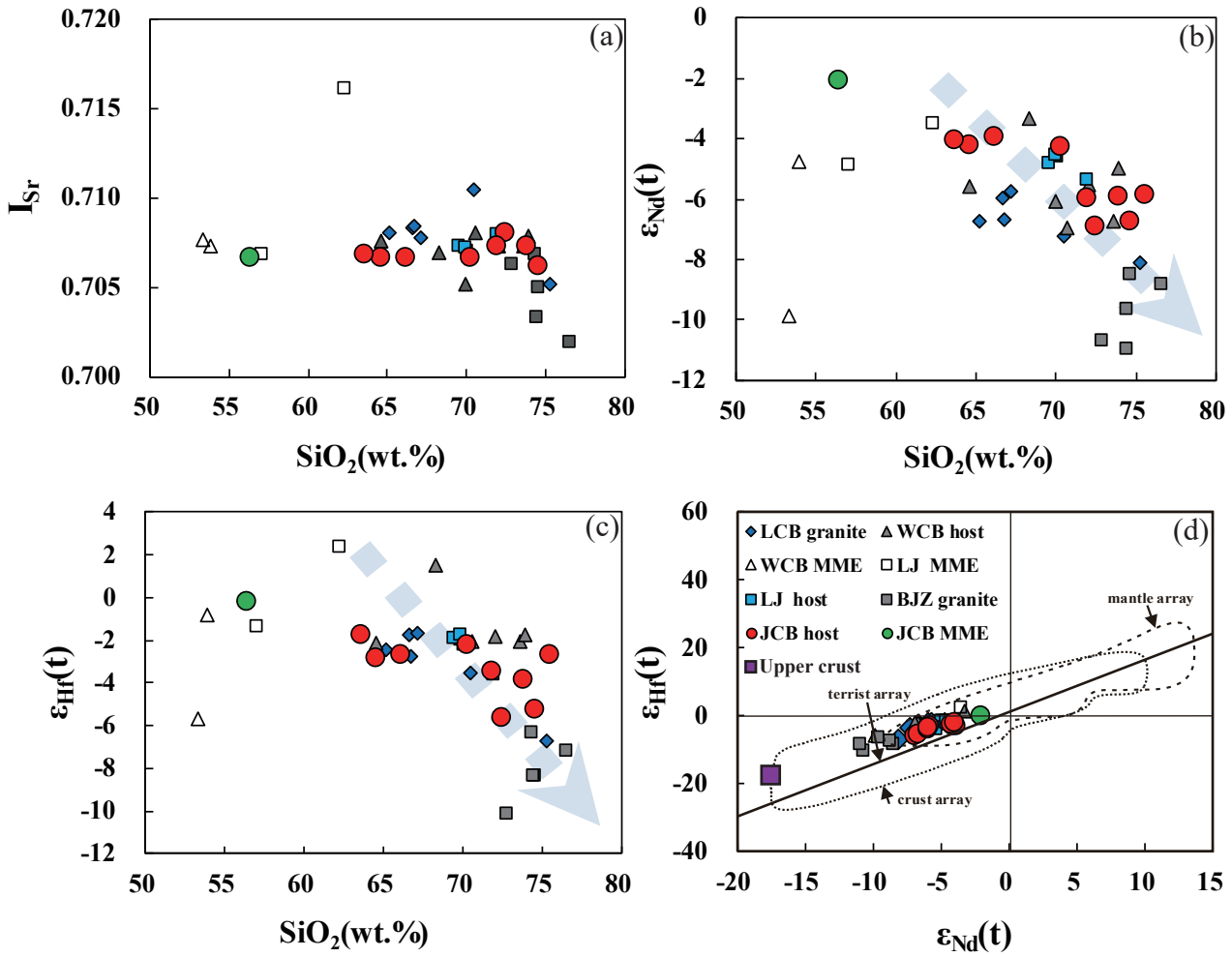
(a)
I_{Sr}
SiO_2(wt.%)
(b)
$\varepsilon_{Nd}(t)$
SiO_2(wt.%)
(c)
$\varepsilon_{Hf}(t)$
SiO_2(wt.%)
(d)
LCB granite
WCB host
WCB MME
LJ MME
LJ host
BJZ granite
JCB host
JCB MME
Upper crust
mantle array
terrist array
crust array
$\varepsilon_{Hf}(t)$
$\varepsilon_{Nd}(t)$

Fig.10

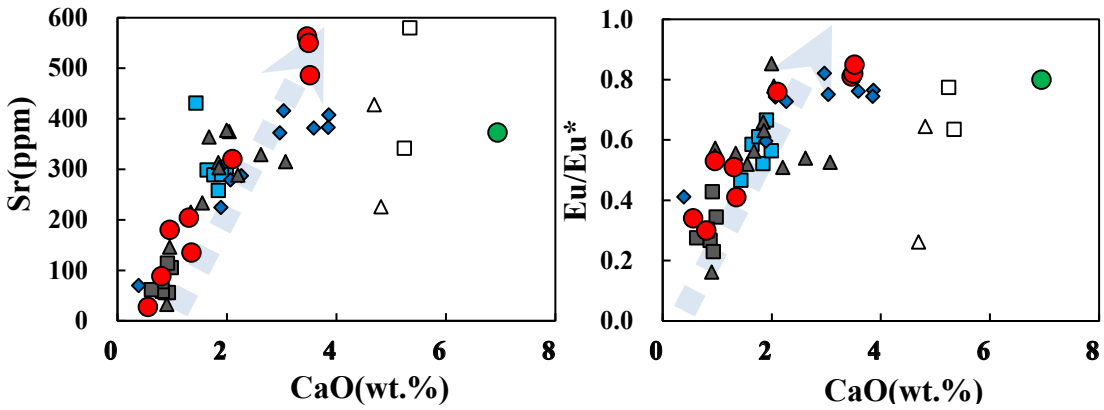
Sr(ppm)
600
500
400
300
200
100
0
0
2
4
6
8
CaO(wt.%)
Eu/Eu*
1.0
0.8
0.6
0.4
0.2
0.0
0
2
4
6
8
CaO(wt.%)

Fig.11

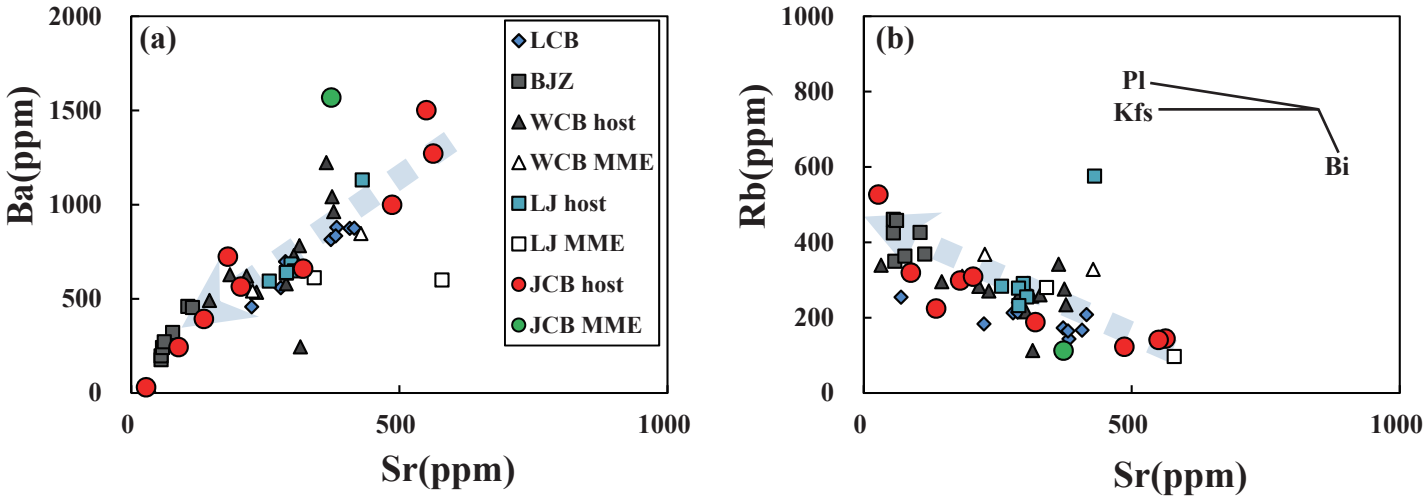
(a)
LCB
BJZ
WCB host
WCB MME
LJ host
LJ MME
JCB host
JCB MME
Ba(ppm)
Sr(ppm)
0
500
1000
1500
2000
(b)
Pl
Kfs
Bi
Rb(ppm)
Sr(ppm)
0
200
400
600
800
1000

Fig.12

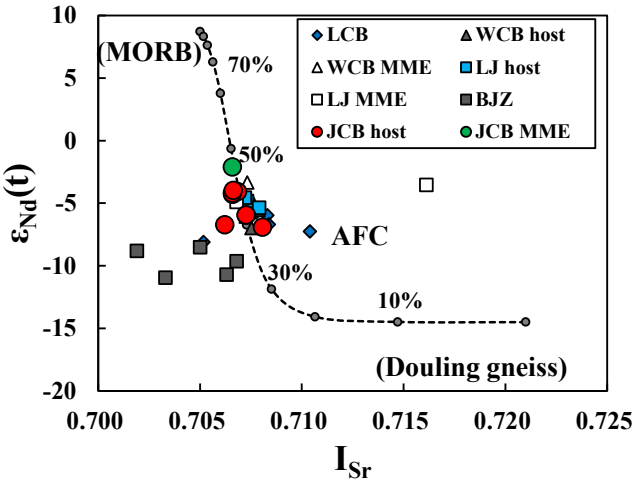
10
5
0
-5
-10
-15
-20
0.700
0.705
0.710
0.715
0.720
0.725
$\varepsilon_{Nd}(t)$
I_{Sr}
(MORB)
70%
50%
30%
10%
AFC
(Douling gneiss)
LCB
WCB host
WCB MME
LJ host
LJ MME
BJZ
JCB host
JCB MME

Fig.13

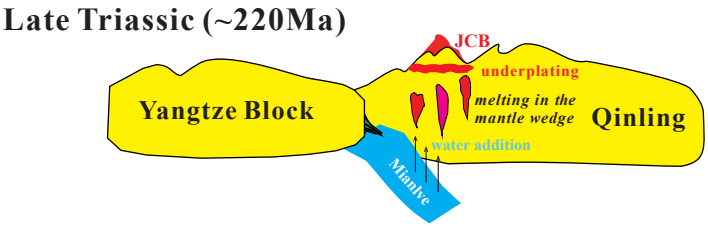
Late Triassic (~220Ma)
JCB
underplating
melting in the
mantle wedge
Yangtze Block
Qinling
water addition
Mianlve